UCLouvain

epl

École polytechnique de Louvain

Modeling the effect of wind shear into a Vortex Particle-Mesh method for wind turbines

Author: **Grégoire CHAPELLE**
Supervisors: **Grégoire WINCKELMANS, Philippe CHATELAIN**
Reader: **Vincent LEGAT**
Academic year 2019–2020
Master [120] in Mechanical Engineering

Abstract

A model for the effect of a shear velocity profile on a wind turbine flow for the Lagrangian vorticity form of the 3-D Navier-Stokes equation is proposed, based on the assumption that vorticity from the shear velocity profile and the turbine do not interact. The model is implemented as part of the Vortex-Particle Mesh method developed by the Thermodynamics and Fluid mechanics Lab at the Universite Catholique de Louvain. Turbines are modeled using the lifting lines method, which is corrected in this work to operate with chosen wind velocity profiles. Simulations of wind turbines operating in linear velocity, power law and atmospheric boundary layer wind profiles are carried out and analyzed in detail. A partial version of the model corresponding to its definition in a 2-D environment is created to study the influence of the model's different terms. The results show that the partial model has little influence on the near wake of the turbine, but slows down the flow below the turbine's hub in the far wake. Reference cases corresponding to the exact phenomenon of a turbine operating under a shear wind profile are created. When compared to the latter, the model yields physically incorrect results. The model produces a flow which generates too much vorticity above hub height and too light below, creating an incorrect upwards deflection of the wake center. An exaggerated power law profile highlights the proportional correlation between the steepness of the profile and the inaccuracy of the model.

Acknowledgements

Ce travail représente le point culminant des mes études en science de l'ingénieur à l'École Polytechnique de Louvain-la-Neuve. J'aimerais exprimer ma gratitude envers toutes les personnes qui m'ont aidé à compléter ce parcours académique, que ce soit les professeurs, les tuteurs ou simplement mes amis. Je tiens surtout à remercier toute personne qui a contribué à la réalisation de mon mémoire de fin d'études.

Je tiens à remercier dans un premier temps mon promoteur, Grégoire Winckelmans, pour son aide et attention malgré le grand nombre de mémorants sous sa supervision. Sa passion et connaissance pour la mécanique des fluides était communicative et motivante.

J'aimerai remercier particulièrement Denis-Gabriel Caprace pour tous ses conseils et son aide au fil de l'année. Sa disponibilité et son implication dans mon travail m'ont été indispensable. Sa volonté à s'assoir avec moi et prendre le temps de discuter des problèmes que comportait le travail a été inestimable. Je tiens également à remercier François Trigaux et Marion Coquelet pour leur volonté à m'aider dans un projet qui ne les impliquait pas directement. Leur aide a été précieuse.

Finalement, j'aimerai remercier mes parents et mes amis pour leur soutien inconditionnel. Ils n'ont jamais manqué à me remonter le moral quand j'en avais besoin, et m'ont encouragé du début jusqu'à la fin.

Contents

Introduction

Today, the production of electricity is based mainly on fossil fuels, namely oil, coal and gas. This unsustainable production of energy is at a turnpoint as temperatures and sea-levels rise. As the world turns to renewable energies, their power capacity is expected to experience a growth of 50% by 2024.[12] Figure 1 illustrates this growth and highlights the need for wind energy : its growth is expected to be the second most important of all the renewable energies, with an expected capacity increase of 750GW.

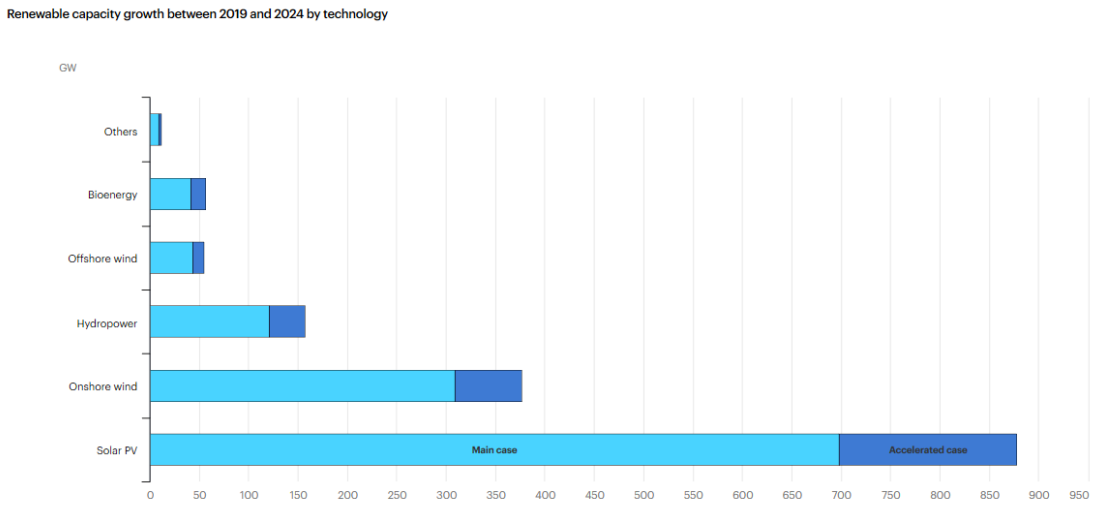

Figure 1: Expected renewable capacity growth between 2019 and 2024.

Wind turbines are one of the fastest-growing energy sources in the world due to their clean energy production and to the overwhelmingly positive results of life cycle assessment methods.[9] While operating, their energy production is free of greenhouse gases and life cycle assessments have proven wind energy production to have one of the lowest CO2 production rates over its lifetime. Wind energy is also plentiful and widespread, allowing for both rural and urban use. Recent technological advancements have made production of energy through wind turbines

competitive with that of fossil fuels.

However, wind turbines are limited by their dependence upon geographic placement and wind conditions. In order to remain competitive with fossil fuels and provide a return on investment, they have to be placed optimally. This implies placing them in remote locations or even offshore, necessitating infrastructural investments to transport the energy to the energy consuming regions. To maximize infrastructural return on investment, the wind turbines are grouped together in wind farms. This compromizes power production efficiency as the wakes of the turbines interfere between each other. Computational tools to simulate wind turbines and their wakes are thus important for their design process.

All wind turbines operate under wind conditions corresponding to that of the local Atmospheric Boundary Layer (ABL). This boundary layer creates a velocity gradient between the no-slip condition at the ground and the free stream velocity outside beyond the boundary layer. Figure 2 illustrates a wind turbine operating in a turbulent atmospheric boundary layer. The characteristics of the ABL have a consequent impact on the power production capacity of wind turbines, and thus must be taken into account during the design stages of the latter.

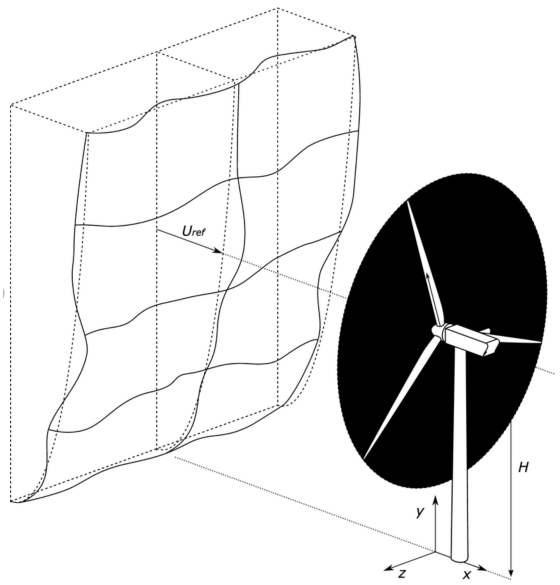

Figure 2: A modern horizontal axis wind turbine operating in a turbulent atmospheric boundary layer. Reprinted from *Large Eddy Simulation of Dynamically Controlled Wind Turbine Arrays*[16].

This thesis aims to study a model for the effect of wind shear velocity profiles on turbines based on the lack of interaction between shear vorticity intrisic to

the shear velocity profile and the vorticity generated by the wind turbine. This model, intitled the *shear effect model*, is paired to an in-house Vortex Particle-Mesh (VPM) Computational Fluid Dynamics (CFD) tool. This method uses Large-Eddy Simulation (LES) to simulate the fluid dynamics and the lifting lines method to model the wind turbine blades.

Neglecting the interaction between the two sources of vorticity allows for the effect of the shear vorticity to exist only as additional terms to the Navier-Stokes (NS) equations instead of being directly interpolated onto particles entering the computational domain. This implies that all zones but the wake of the turbine are devoid of vorticity. In vortex-particle methods, this could prove to cut down computational costs. This study assesses the functioning and the accuracy of such a model.

Simulations will be performed with various profiles and boundary conditions with the objective of quantifying the behaviour of the wake in terms of velocity and vorticity.

Chapter 1 This chapter briefly describes the VPM method used in this work. The theory and incorporation of the *shear effect model* into the NS equations will then be presented, as well as the adjustments made to the lifting lines method for it to remain physically coherent.

Chapter 2 Comparisons of simulations performed with and without the shear effect model will be presented. The aim of this chapter is to gain a better understanding of which terms of the model within the NS equations are predominant, all the while seperating the effects of a correction applied to the lifting lines method. A partial version of the model will be presented to highlight the influence of the term suspected to be predominant.

Chapter 3 This chapter will compare simulations ran with the shear effect model to simulations ran with physically accurate shear velocity profile modeling, where the shear vorticity is interpolated directly onto particles entering the domain. These cases do not neglect the interaction of shear vorticity and vorticity generated by the turbine and thus will be critical to determine the accuracy of the shear effect model.

Chapter 1

Aerodynamic Solver

This first chapter will present the theoretical background as well as the numerical tools used to perform the simulations and model the effect of shear vorticity. First, the vorticity-velocity formulation of the Navier-Stokes equations will be presented, then its numerical solver, the VPM method, will be thoroughly presented.

The interested reader can refer to [5], [6] and [17] for more information on the VPM solver.

Contents

1.1 Vorticity-velocity formulation of the Navier-Stokes equations

The Navier-Stokes equations describe the motion of viscous fluid substances through a set of Partial Differential Equations (PDEs) arising from the application of Newton's second law. These equations represent the conservation of mass, momentum and energy of Newtonian fluids. The mass and momentum equations are :

$$\frac{\partial \rho}{\partial t} + \nabla \cdot (\rho \mathbf{u}) = 0 \tag{1.1}$$

$$\rho(\frac{\partial \mathbf{u}}{\partial t} + \mathbf{u} \cdot \nabla \mathbf{u}) = -\nabla p + \mu \nabla^2 \mathbf{u} + \frac{1}{3}\mu \nabla(\nabla \cdot \mathbf{u}) + \rho \mathbf{g} \tag{1.2}$$

By making the assumption that the flow is incompressible ($\frac{\partial \rho}{\partial t} = 0$), that there are no external sources ($\mathbf{g} = 0$) and by dividing both sides of the equations by ρ, they become :

$$\nabla \cdot \mathbf{u} = 0 \tag{1.3}$$

$$\frac{\partial \mathbf{u}}{\partial t} + \mathbf{u} \cdot \nabla \mathbf{u} = -\nabla P + \nu \nabla^2 \mathbf{u} \tag{1.4}$$

where ν is the kinematic viscosity, a measure of the inherent resistance of a fluid to flow. These equations represent the velocity-pressure form of the equations. By taking the curl of the equation (1.4), the vorticity-velocity form is obtained.

$$\frac{\partial \boldsymbol{\omega}}{\partial t} + (\nabla \boldsymbol{\omega}) \cdot \mathbf{u} = (\boldsymbol{\omega} \cdot \nabla)\mathbf{u} + \nu \nabla^2 \boldsymbol{\omega} \tag{1.5}$$

with $\boldsymbol{\omega} = \nabla \times \mathbf{u}$ by definition. This definition implies that the divergence of vorticity is always equal to zero.

$$\nabla \cdot \boldsymbol{\omega} = \nabla \cdot (\nabla \times \mathbf{u}) = 0 \tag{1.6}$$

This means that vortex filaments, connected vortex points of same magnitude, must either form a closed vortex ring, or must terminate at the fluid boundary. This is the **solenoidal** property, a property that must always be respected. The numerical schemes discretizing the Navier-Stokes equations must oblige by that rule. Since the different forms of these equations will govern which discretization schemes are used, they will yield different inconsistencies.

Applying a Helmholtz decomposition, the velocity field can be resolved into the sum of an irrotational velocity field and a the solenoidal velocity field $\mathbf{u} = \mathbf{u}_\omega + U_\infty$.

The combination of these previous two relations allows for the recovery of the velocity field by solving the Poisson equation

$$\nabla^2 \mathbf{u}_\omega = -\nabla \times \boldsymbol{\omega} \tag{1.7}$$

1.2 The Vortex Particle-Mesh method

Solutions to the Navier-Stokes equations are used in many practical applications, most notably in the field of fluid dynamics. However, the existence and unicity of a solution to these equations has not yet been demonstrated. Approximations of the solution have been reached using models and numerical computation.

An aerodynamic solver using the VPM method has been developped by the Thermodynamics and Fluid mechanics Lab (TFL) at the Universite Catholique de Louvain (UCL). The VPM method is the combination of a vortex particle method and a mesh.

The vortex particle method is used to handle the advection of vorticity in a Lagrangian fashion. This method is useful for convection-heavy turbulent flows.

Mesh-based methods are efficient at numerically computating differential operators and solvers for the Poisson equation.

This combination makes for very efficient computation of insteady and incompressible flows. Furthermore, this solver runs on Massively Parallel Architectures (MPI).

1.2.1 The Vortex Particle method

The Vortex Particle method relies on the discretization of the vorticity field into particles that have an assosciated position $\mathbf{x_p}$, strength $\boldsymbol{\alpha_p}$ and volume V_p. The strength is a measure of vorticity of the particle, defined as the volume integral of the vorticity:

$$\boldsymbol{\alpha_p} = \int_{V_p} \boldsymbol{\omega} d\mathbf{x} \simeq \boldsymbol{\omega_p} V_p \tag{1.8}$$

where $\boldsymbol{\omega_p}$ represents the average vorticity magnitude of the volume V_p. The global vorticity function can then be defined by using a distribution function ξ_p for each particle.

$$\boldsymbol{\omega}(\mathbf{x}, t) = \sum_p \boldsymbol{\alpha_p} \xi_p(\mathbf{x} - \mathbf{x_p}(t)) \tag{1.9}$$

This definition of vorticity takes into account the contribution of all the particles. Unlike mesh methods, the data points are not restricted to a grid. Instead, they move around freely with the flow, their assosciated vorticity varying with respect to position and time. The following Ordinary Differential Equations (ODEs) govern the evolution of the particles' positions and assosciated strengths.

$$\frac{d\mathbf{x_p}}{dt} = \mathbf{u_p} = \mathbf{u}(\mathbf{x_p}, t) \tag{1.10}$$

$$\frac{d\boldsymbol{\alpha_p}}{dt} = \int_{V_p} [(\boldsymbol{\omega} \cdot \nabla)\mathbf{u} + \nu\nabla^2\omega]d\mathbf{x} \simeq [(\boldsymbol{\omega} \cdot \nabla)\mathbf{u} + (\mathbf{x_p} + \nu\nabla^2\boldsymbol{\omega}(\mathbf{x_p}))]V_p \tag{1.11}$$

Equation (1.11) is obtained by the combination of the definition of particle strength (1.8) and the vorticity-velocity form of the Navier-Stokes equations (1.5). The particle strength thus undergoes vortex stretching and diffusion.

These ODEs make for a simple but efficient implementation. The vorticity-velocity form being devoid of a convection term, it does not require its discetization. Therefore, the method does not require the CFL condition. Furthermore, the lack of explicit integration schemes for advection allows for larger time steps. However, using Lagrangian formulation for flows under very excessive deformations can lead to large distortions of the elements, which in turn increases the computational time and inaccuracies. These particles will tend to accumulate in certain regions of the flow, leaving other regions scarce in particle density. Finally, solving the Poisson equation (1.7) is very computationally intensive, as it is an elliptic problem. Green's solution to this problem is more costly than other mesh-based solvers.

1.2.2 Combining a mesh-based approach

The VPM method attempts to solve these problems by periodically remeshing the particles onto a grid using high-order interpolation methods.

$$\boldsymbol{\alpha_p} = \sum_p \boldsymbol{\alpha_p} W(\frac{\mathbf{x_q} - \mathbf{x_p}}{h}) \tag{1.12}$$

where $\mathbf{x_q}$ denotes the particles' positions on the mesh. W represents the interpolation kernel required to compute the strength values of the newly remeshed particles and h the mesh spacing. The mesh is also used to increase the time steps, as the method is no longer strictly Eulerian, resulting in improved computational efficiency.

After the remeshing interpolation is computed, finite discretization schemes can easily be performed to evaluate the various differential operators and quantities.

The mean vorticity magnitude is computed applying the same logic than for particle strength:

$$\boldsymbol{\omega_q} = \sum_p \frac{\boldsymbol{\alpha_p}}{h^d} W(\frac{\mathbf{x_q} - \mathbf{x_p}}{h}) \tag{1.13}$$

where d is the interpolation method's order. The mesh allows for the use of faster solvers to the Poisson equation (1.7). Once the Poisson equation has been solved, the **solenoidal** condition has to be guaranteed by reconnecting the vortex filaments. This step is necessary as the vortex particle method generates divergence. It is performed with a relaxation process in Fourier space. The quantities are then interpolated back onto the particles. The VPM method revolves around alternating interpolation processes between particles and mesh. Finally, a low storage Third Order Runge-Kutta (RK3) scheme is used to perform the time-integration step.

1.2.3 Bodies in the flow

The VPM method used in the context of this work can simulate the effect of bodies in the flow through the use of immersed Prandtl's lifting-lines. These bodies are typically slender lifting bodies such as airplane wings and wind turbine blades. The immersed lifting-lines generate vorticity, modeling the bodies.

Prandtl's lifting-line theory The Prandtl lifting-line theory predicts the evolution of lift distribution over the wing. It applies the concept of circulation and the Kutta-Joukowski theorem under the assumption of steady flows. Circulation is the contour integral of the velocity:

$$\Gamma = -\oint_{\partial S} \mathbf{u} \cdot d\mathbf{l} = -\int_S \boldsymbol{\omega} \cdot \mathbf{n} dS \tag{1.14}$$

This implies that the bound circulation around infinitesimal airfoil section determines the strength of its attached vorticity. The circulation is related to the lift per unit span:

$$L = \rho U_{rel} \Gamma \tag{1.15}$$

where U_{rel} is the relative velocity. The concept of the lifting line is to model an airfoil with a vortex filament, going through each wing section. The second Helmoltz theorem states that a vortex filament must be closed and cannot finish in the fluid, thus implying that the lift of an element creates a closed loop of constant circulation. However, when the airfoil is in motion, the loop closes far in its wake, allowing the effect of its induced velocities on the airfoil to be overlooked.

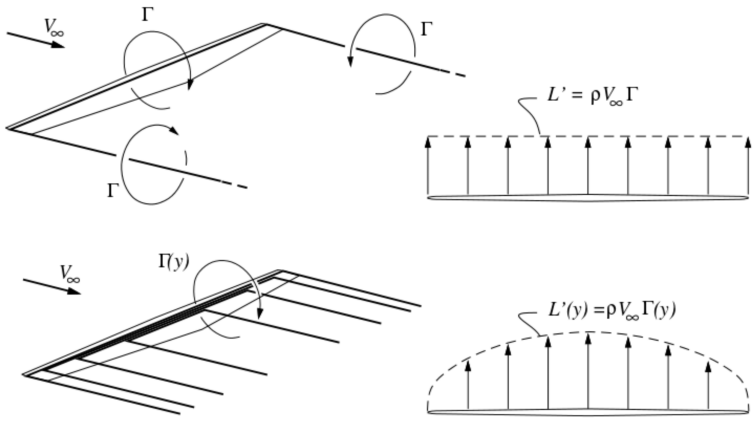

Figure 1.1: Vortex Arrangement for the Prandtl Lifting-Line Theory. Reprinted from *Multiple-Wake Vortex Lattice Method for Membrane-Wing Kites*[14]

For constant circulation, a horseshoe vortex is obtained. Since the wing is finite, it cannot produce lift at its tips and thus the local circulation must be equal to zero. Elsewhere along the wing, lift is produced thus circulation is not equal to zero. One can consider a wing to be a combination of infinitesimal airfoil sections with assosciated vortices of different strengths, implying a circulation distribution along the span of the wing (see figure 1.1).

Kelvin's circulation theorem states that in a barotropic ideal fluid with conservative body forces, the circulation around a closed curve (which encloses the same fluid elements) moving with the fluid remains constant with time $\frac{D\Gamma}{Dt} = 0$. There is no free stream velocity for a fluid at rest, thus no circulation and lift. Since Kelvin's theorem states that circulation must be conserved, any temporal variation of this value must be counteracted. The initial acceleration thus induces a **starting vortex**. The theorem also acts upon spatial variations, meaning that the circulation distribution along the wing will shed vortices, resulting in a vortex sheet.

Applying the lifting-line theory When coupled with the Kutta-Joukowski condition, the lifting-line theory yields equation (1.15), allowing for the computation of the airfoil performance for a defined circulation distribution. In the VPM code, this concept is reversed in order to deduce the circulation distribution from the aerodynamic coefficients of the bodies given as input. Indeed, the aerodynamics polars of the airfoil are given, providing the values of the lift and drag coefficients C_L and C_D, as a function of the angle of attack. The value of the chord-based Reynolds number is also provided, allowing for the computation of lift on each wing

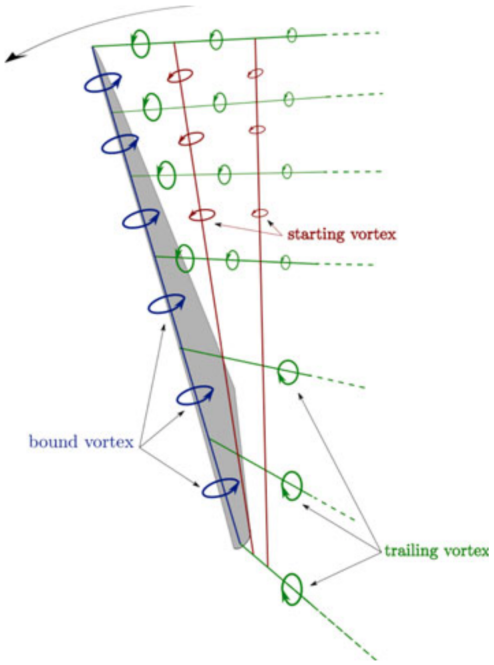

Figure 1.2: Vorticity sources modeled through a lifting line approach for a rotating blade. Reprinted from *Vortex Particle-Mesh with Immersed Lifting Lines for Aerospace and Wind Engineering*[1]

.

section. The assosciated bound circulation distribution $\Gamma(y,t)$ can then be computed. Applying the **solenoidal** property then allows to determine the vortex sheet.

The last step for lifting-lines to be a complete representation of the sources of vorticity is to include the trailing vortices (see figure 1.2). This is done by discretizing the bound vortex in a different set of vortex particles then using the already existing particle-mesh methods to interpolate the velocity field onto the particles. Lagrangian tracers are then placed along the lifting line to construct the shed vorticity in a vortex lattice fashion. This takes into account the spatial and temporal variations of the circulation Γ. These tracers allow for the computation of the shed vortex sheet at any time-step, useful for multistep time integration schemes. Unlike the actuator line technique, this method allows for large time steps unrestricted by the blade tip speed. Finally, the shed vorticity is then interpolated from the new vortex particles onto the particles of the bulk flow.

It is worth noting that the Kutta-Joukouwski is originally derived for a steady potential two-dimensional flow. However, it has been shown that it also applies to a separated flow in a time-averaged sense [18].

Extracting aerodynamic performances In the VPM code, the lifting bodies are represented by lifting lines and given as input in the form of text files containing the aforementioned aerodynamic polars, geometric dimensions as well as orientations. These bodies can have associated angular velocities, useful in the case of rotating bodies such as wind turbines. The aerodynamic performances along the lifting-line sections are produced and retrieved in data files. Among others, the power, torque, position of the blades, angle of attack, lift and drag forces are dumped at every time-step, for every body.

1.2.4 Large Eddy Simulation

The wake of a wind turbine is typically a complex turbulent flow, requiring intense computational cost to resolve at all scales. LES is a mathematical model that reduces this cost by ignoring the smallest turbulence scales, which are the most computationally expensive to resolve. It applies low-pass filtering to the Navier-Stokes equations, then models the effect of the ignored small scales with a Sub-Grid Scale (SGS) model. The Lagrangian vorticity form of the Navier-Stokes equation (1.5) can also perform LES [7].

$$\frac{D\boldsymbol{\omega}}{Dt} = (\boldsymbol{\omega} \cdot \nabla)\mathbf{u} + \nu\nabla^2\boldsymbol{\omega} + \nabla \cdot \mathbf{T}^M \tag{1.16}$$

where $\mathbf{T}^M$ is the SGS model, designed as an eddy viscosity model acting only on the small-scale field

$$\mathbf{T}^M = \nu_{SGS}(\nabla\boldsymbol{\omega}^s - (\nabla\boldsymbol{\omega}^s)^T) \tag{1.17}$$

where $\boldsymbol{\omega}^s$ represents the small-scale part of the vorticity field obtained by high-pass filtering. The eddy viscosity is taken as $\nu_{SGS} = C_r^{(n)}\Delta^2(2\mathbf{S} : \mathbf{S})^{1/2}$. The interested reader can refer to Cocle *et al.* [8] and D.-G. Caprace *et. al.* [4] for implementation details.

1.2.5 Representation of Shear in the Navier-Stokes equations

The viscosity term $\nu\nabla^2\boldsymbol{\omega}$ is very small in the context of this thesis and the SGS term $\mathbf{T}^M$ acts as part of a numerical model. For the sake of clarity, these terms are not displayed in the equations of the following sections, despite being present in the VPM code. We now consider a vertical shear profile $\mathbf{U} = U(z)\mathbf{e}_x$ that induces a vorticity profile $\boldsymbol{\Omega} = \nabla \times \mathbf{U} = \frac{dU}{dz}(z)\mathbf{e}_y = \Omega(z)\mathbf{e}_y$.

Shear only Applying this shear profile to the vorticity-velocity formulation yields:

$$\frac{\partial \mathbf{\Omega}}{\partial t} + (\nabla \mathbf{\Omega}) \cdot \mathbf{U} = (\nabla \mathbf{U}) \cdot \mathbf{\Omega} \tag{1.18}$$

For a uniform and steady flow, $\frac{\partial \mathbf{\Omega}}{\partial t} = 0$, $(\nabla \mathbf{\Omega}) \cdot \mathbf{U}$ and $(\nabla \mathbf{U}) \cdot \mathbf{\Omega} = 0$.

Shear and additional vorticity In the case where another source of vorticity is present in the flow, the total vorticity is $\boldsymbol{\omega}_{tot} = \boldsymbol{\omega} + \mathbf{\Omega}$ and the total velocity is $\mathbf{u}_{tot} = \mathbf{u} + \mathbf{U}$. The substitution of these profiles into equation (1.5) is given below:

$$\frac{\partial}{\partial t}(\boldsymbol{\omega} + \mathbf{\Omega}) + (\nabla(\boldsymbol{\omega} + \mathbf{\Omega})) \cdot (\mathbf{U} + \mathbf{u}) = (\nabla(\mathbf{U} + \mathbf{u})) \cdot (\boldsymbol{\omega} + \mathbf{\Omega}) \tag{1.19}$$

If the assumption that the additional vorticity does not interact with the shear vorticity is made, subtracting equation (1.18) from equation (1.19) yields:

$$\frac{\partial \boldsymbol{\omega}}{\partial t} + (\nabla \mathbf{\Omega}) \cdot \mathbf{u} + (\nabla \boldsymbol{\omega}) \cdot (\mathbf{U} + \mathbf{u}) = (\nabla \mathbf{u}) \cdot \mathbf{\Omega} + (\nabla(\mathbf{U} + \mathbf{u})) \cdot \boldsymbol{\omega} \tag{1.20}$$

$$\frac{D\boldsymbol{\omega}}{Dt} = (\nabla(\mathbf{U} + \mathbf{u})) \cdot \boldsymbol{\omega} - (\nabla \mathbf{\Omega}) \cdot \mathbf{u} + (\nabla \mathbf{u}) \cdot \mathbf{\Omega} \tag{1.21}$$

Further decomposing this equation yields the following system of equations:

$$\frac{D}{Dt}\omega_x = \frac{\partial u}{\partial x}\omega_x + \frac{\partial u}{\partial y}\omega_y + \frac{\partial u}{\partial z}\omega_z + \frac{\partial U}{\partial z}\omega_z + \frac{\partial u}{\partial y}\Omega \tag{1.22}$$

$$\frac{D}{Dt}\omega_y = \frac{\partial v}{\partial x}\omega_x + \frac{\partial v}{\partial y}\omega_y + \frac{\partial v}{\partial z}\omega_z - \frac{\partial \Omega}{\partial z}w + \frac{\partial v}{\partial y}\Omega \tag{1.23}$$

$$\frac{D}{Dt}\omega_z = \frac{\partial w}{\partial x}\omega_x + \frac{\partial w}{\partial y}\omega_y + \frac{\partial w}{\partial z}\omega_z + \frac{\partial w}{\partial y}\Omega \tag{1.24}$$

It can be observed that the terms added by the model are all dependent of the first and second derivatives of the wind velocity profile. This implies that the model works independentely from the magnitude of velocity of the flow; it is only influence by the rate at which the velocity changes over a certain distance. Furthermore, the presence of first and second derivatives means that for similar values, linear and non-linear wind velocity profiles are expected to behave differently.

The set of equations brings to light the fact that every term is a factor of vorticity or the first derivative of velocity. In other words, the model will only act within the wake of the turbine.

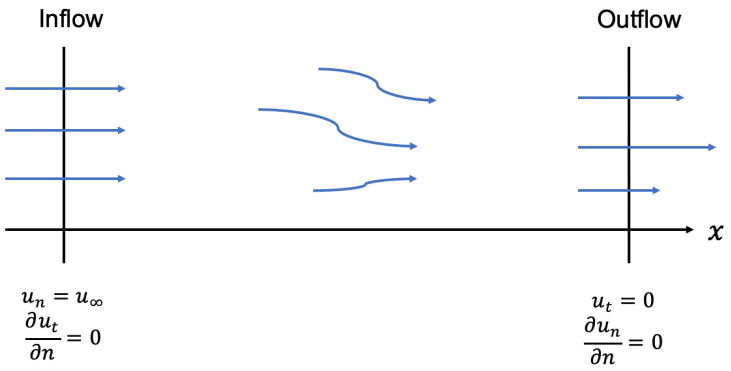

Figure 1.3: Boundary conditions at the inflow and outflow.

Inflow-outflow conditions The inflow-outflow conditions are defined in figure 1.3. They represent a uniform flow at the inflow of the computational domain that undergoes a perturbation (in this case due to the wind turbine). The flow exits the domain with non-uniform velocity in the streamwise direction.

1.2.6 Implementation

Since the model only acts as additional terms to the NS equations (1.5), their implementation is straightforward. Indeed, if a wind velocity profile is given as input, these terms are added to the Lagrangian derivative after the computation of the right hand side of equation (1.5) in the VPM code.

Three methods of reading a shear velocity profile have been implemented in the context of this thesis. They are passed as input in one of the following ways:

- One ".dat" file corresponding to the shear velocity profile $U(z)$. The profile must be discretized corresponding to the mesh of the vertical direction. If this is not the case, the execution stops and an error message is sent. Two ghost points are extrapolated on each side of the domain in order to perform a numerical derivation of the fourth order to retrieve the velocity gradient $\frac{dU}{dz}(z)$. This step is repeated to retrieve the second derivative $\frac{d^2U}{dz^2}(z) = -\frac{d\Omega}{dz}(z)$.

- Two or more ".dat" files corresponding to the wind velocity profile $U(z)$ and optionally its derivatives $\frac{dU}{dz}(z)$ and $\frac{d^2U}{dz^2}(z)$. This avoids relying on extrapolation schemes to generate the necessary ghost points required to compute the first and second derivatives, thus reducing error.

- The coefficients of analytical equations representing various velocity profiles, allowing for analytical derivation and thus entirely avoiding error in numerical

derivation and extrapolation.

A parameter defining the domain on which the model acts was also implemented. This is necessary to prevent the model from operating at the point on the x-axis where the blades are. The model is not meant to accurately operate near the zone where the lifting lines are generated; it would only create unwanted interference. In all of the simulations, the model begins operation three meters in the wake of the wind turbine.

1.2.7 Staying consistent with the lifting lines theory

Since VPM uses the aerodynamic polar and the wind velocity to determine the lift, which in turn is used to determine the circulation, the wind velocity gradient must be taken into account in this calculation. The shear velocity profile given as input is thus interpolated onto the lifting line particles of the blades of turbine and then used to compute lift, while the particles upstream of turbine maintain a uniform velocity field that corresponds to the free-stream velocity (figure 1.4).

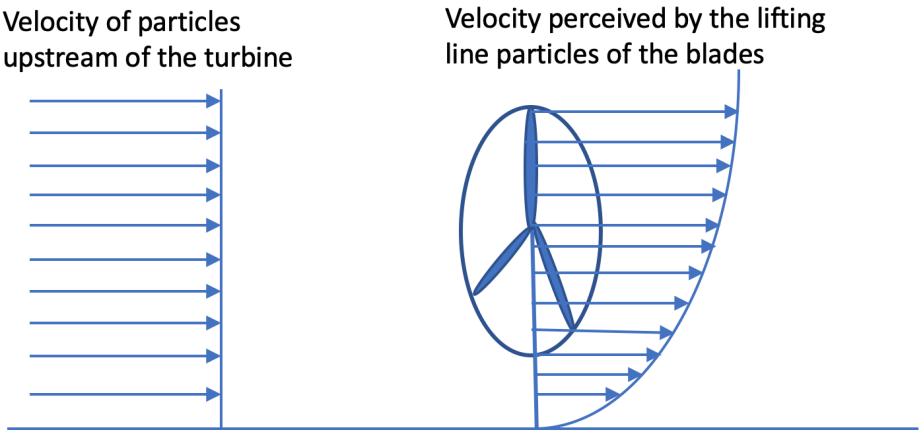

Figure 1.4: Velocity field upstream of the turbine versus the field the lifting lines particles use to compute circulation.

Chapter 2

Model behaviour

Chapter 1 presented the details of the VPM code to give context to the inner workings of the simulations presented in the following sections. It also provided the mathematical and physical explanation of the shear model.

This chapter seeks to evaluate the effect of the model on the flow when the wind turbine undergoes linear and power law wind velocity profiles. To do so, a comparison is established between the case without the model, with a partial version of the model and with its complete version.

Contents

2.1 Linear wind profile

Throughout this thesis, the way the shear effect model reacts to linear and non-linear wind profiles will be examined. In order to create relevant comparisons between these cases, the profiles have to be chosen carefully. The profiles have to be as equivalent as possible while maintaining their linear and non-linear properties. For this reasion, the linear profile will be computed from a least squares linear regression applied to an atmospheric boundary layer model: the power law (described in section 2.1.3).

2.1.1 Computational setup

The computational domain used in the present study has dimensions $8D \times 2D \times 3D$ as shown in Figure 2.1. The wind turbine used as reference is the NREL-5MW offshore wind turbine, described more thoroughly in [13]. It has a diameter D of 126m and its hub is 90m high. The boundary conditions are inflow and outflow at $x = -1.5D$ and $x = 6.5D$ respectively (section 1.2.4). Unbounded boundary conditions are initially imposed at $z = 0D$ and $z = 3D$. The upstream velocity is set at 5.79m/s with the angular velocity of the rotor being 7.8 RPM. This yields a tip-speed ratio of $\lambda = 8.89$. The grid resolution is of 64 points per diameter in each direction. The time step δt is adaptative and initially set to its maximum value of 0.192s. The timestep can decrease when needed but not exceed the maximum value. The simulation is performed over 250 seconds, which is equivalent to 1.5 convective times. The flow statistically converges at around 200 seconds, after 1.15 convective times. Statistics are then computed on the last 46 seconds, from $t = 204$ to $t = 250$, representing 6 revolutions.

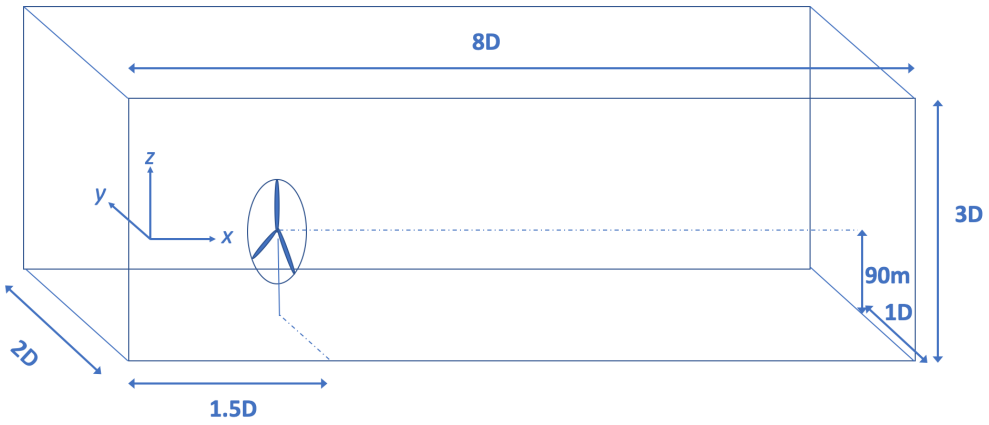

c

Figure 2.1: Computational setup for the linear shear wind profile.

2.1.2 Boundary conditions

The VPM allows for the use of periodic and unbounded boundary conditions in the y and z directions. For the linear velocity profile simulations, we impose unbounded boundary conditions in these directions. The unbounded boundary conditions increase the domain size in chosen directions when the vorticity at the domain boundaries reaches a chosen threshold. This allows for leakage through these interfaces while maintaining the computational efficiency of a smaller initial domain size. The unbounded boundary conditions are transverse to the streamwise direction.

2.1.3 Velocity profile

In this first series of simulations, the wind turbine is going to be exposed to a wind velocity profile corresponding to the power law. This law is given by the following equation:

$$\frac{U}{u_h} = \left(\frac{z}{z_h}\right)^{\alpha} \tag{2.1}$$

where u_h represents the velocity of the wind at the wind turbine's hub, z_h its height and α is an empirically derived coefficient. This coefficient is expressed as a fraction $\alpha = \frac{1}{n}$ where n is typically 8-10 for high Reynolds flows. This coefficient is thus set to $\alpha = \frac{1}{9}$.[11] The linear regression used to compute the linear velocity profile is applied only in the zone where the model has the most impact. Since the model only acts upon areas where vorticity already exists, it can be assumed that the model almost exclusively acts upon the wake of the turbine. Therefore, the linear regression is performed between the points where the tip of a blade is at its highest and lowest in a rotation. The velocity profiles that correspond to the case where the hub velocity is $u_h = 5.79$m/s and the hub height is $z_h = 90$m are plotted in figure 2.2.

The linear regression yields the following linear velocity profile:

$$U(z) = 0.0079z + 5.0238 \tag{2.2}$$

This profile is then used to create the linear wind profile simulations.

2.1.4 Results and discussion

The aim of this section is to grasp a better unstanding of how the terms added to the Navier-Stokes equations influence the behaviour of the flow. To assess this, side-by-side comparisons of the VPM simulations with and without the model are presented. The data will be represented in the following formats:

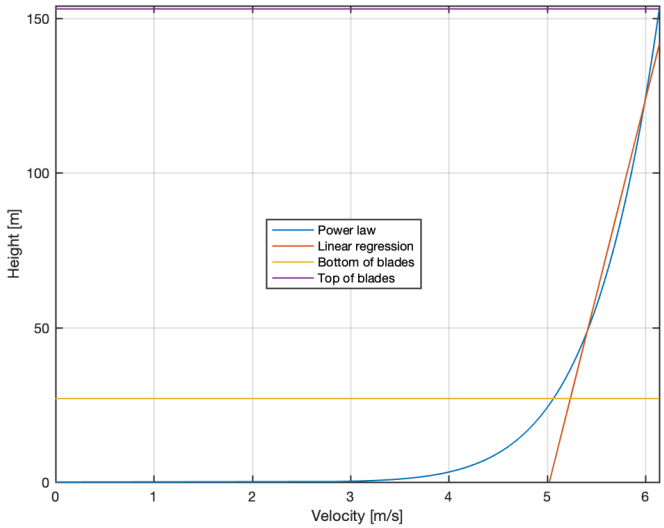

Figure 2.2: Linear wind velocity profile from a linear regression on the power law

- 3D instantaneous snapshot of the vorticity.
- 2D instantaneous slice of the normalized vorticity.
- Time-averaged slices of streamwise velocity in different planes.
- Time-averaged velocity deficit in the wake at various positions.

The computational setup for all cases is such that the height of the turbine's hub is 90m. However, it is important to note that, in this case, there is no wall or no-slip condition 90m below the hub. This altitude only quantifies the position of the turbine with respect to the computational box. The flow can and will leak below $z = 0$. This case is purely theoretical and used to display the effects of the model.

Effects of the profile perceived by the lifting lines

In order to grasp the way the model acts on the flow, it is important to separate its effects into two categories: The ones created by the lifting lines method acting upon the velocity profile sought to be modeled and the ones created by the additional terms of the RHS of the velocity-vorticity formulation of the NS equations. Figure 2.3 depicts the time-averaged streamwise velocity deficits at various positions in flows with and without the linear velocity profile applied to the lifting lines method. In this case, the additional shear effect model terms of the NS equations have not

yet been added. This is done in an attempt to grasp a better understanding of what proportion of the effects of the model are due to the vorticity generation of the lifting lines.

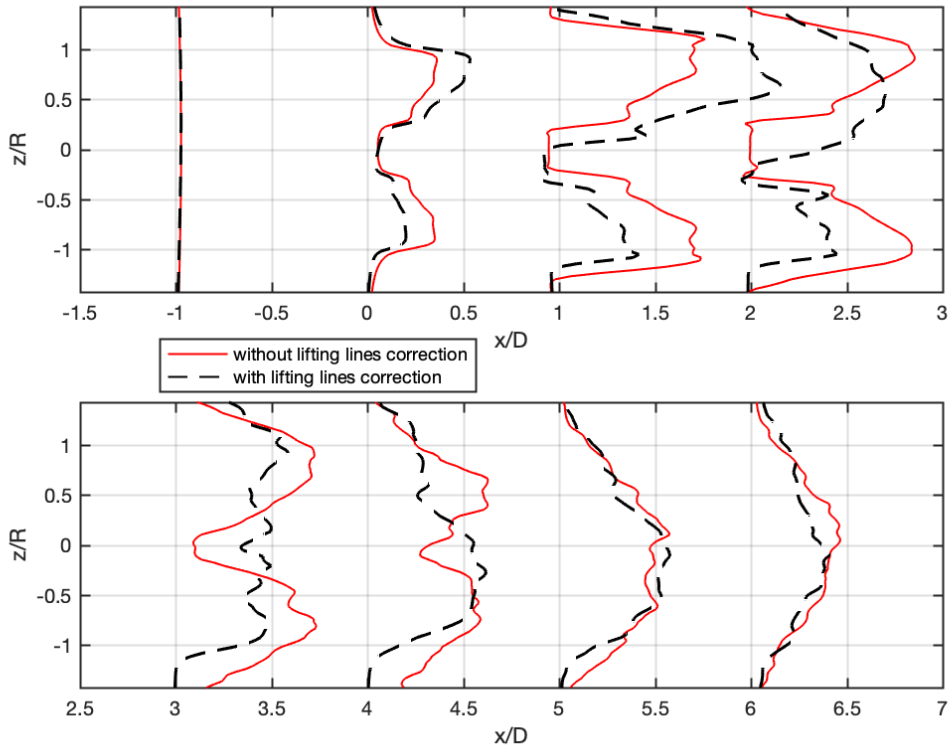

Figure 2.3: Time averaged velocity deficit $\frac{U_\infty - u_x}{U_\infty}$ with and without lifting lines correction.

At $x/D = 0$, the effect of the velocity profile perceived by the lifting lines method is apparent. The velocity deficit is greater above the hub and smaller below the hub. The difference in velocity of these two regions is a combination of the perceived velocity in the lifting lines method with the uniform velocity of the particles upstream from the turbine. The blades at the top will thus shed more vorticity while the blades at the bottom will shed less. Since the velocity field of the particles is actually uniform, the shed vorticity generated by the lifting lines method will not be compensated by a corresponding vorticity field associated to the particle velocity field perceived by the blades. The wake center, represented by the local velocity minima, is deviated downwards. It can be observed that the maximum velocity deficit at $x/D = 0$ is much greater for the case with lifting lines correction. However, the greater shed vorticity has the effect of mixing the

flow above the hub, rapidly decreasing this local maximum. At $x/D = 2$, the maximum velocity deficit without lifting lines correction becomes greater than its counterpart with correction. This mixing phenomenon can also be observed with the disappearance of the wake center: the local velocity deficit minimum disappears at $x/D = 3$ for the case with correction, whereas it disappears at $x/D = 5$ without. Finally, the figure highlights how the wake near $z = 0$ spreads less with correction due to the fact less vorticity is shed by the blades beneath the hub.

The following sections will now seek to highlight the effects of the additional shear effect model terms of the RHS of the velocity-vorticity formulation of the NS equations.

Instantaneous vorticity snapshots

Figure 2.4 displays the iso-contours of vorticity in the wake of the NREL-5MW wind turbine for the VPM method and VPM method with shear effect modeling. The wake of a wind turbine can be characterised in three parts: First, vortex tubes are generated by the tips of the blades. These vortex tubes are characterised by their separation from one another. They here progressively evolve into an "almost continuous" vortex sheet that eventually becomes unstable due to Kelvin-Helmholtz instabilities. This causes the sheet to become turbulent [10],[2].

The wake of the VPM simulation with shear effect modeling evolves much sooner into its turbulent state. The wake is more chaotic and there is more saturation in the colormapping of vorticity. As can be expected, the shear effect model generates more vorticity in the flow. As seen in equations 1.22, the model acts exclusively in areas where vorticity is already present and amplifies it.

Figure 2.5 displays slices of the y-vorticity, normalized using a factor $\frac{D}{U_\infty}$. Looking at the wake structure, one can immediately observe that the lifting lines correction has a much more significant impact on the shape of the flow than the additional terms of the NS equations. The two flows barely deviate and share a similar asymmetrical structure between the bottom and the top of the wake. The values of the vorticity generated by the blades are approximately equivalent.

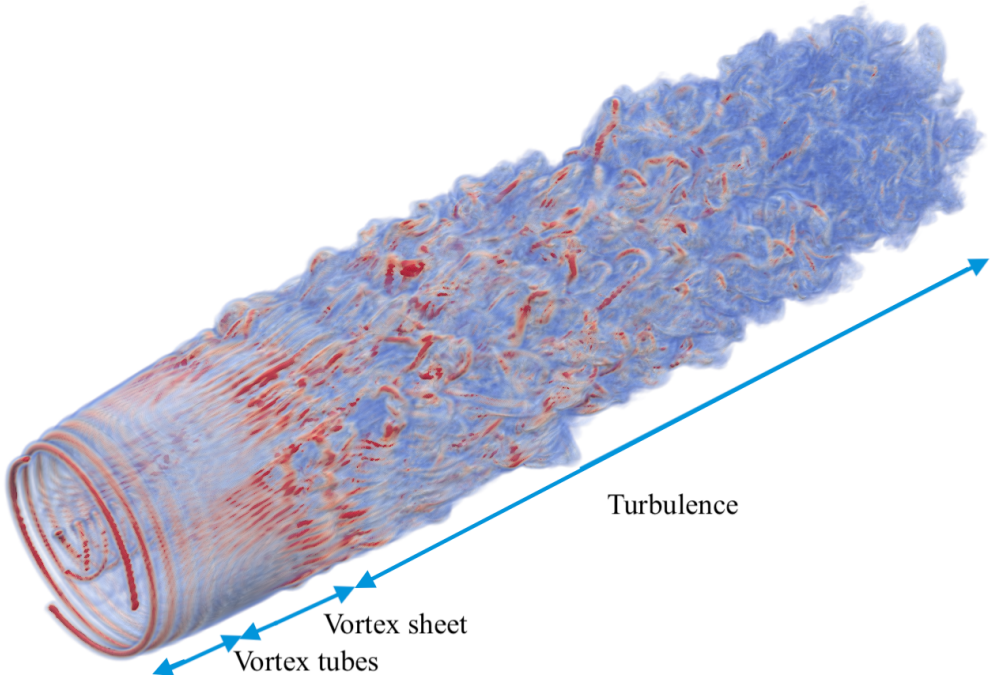

(a) unmodified VPM

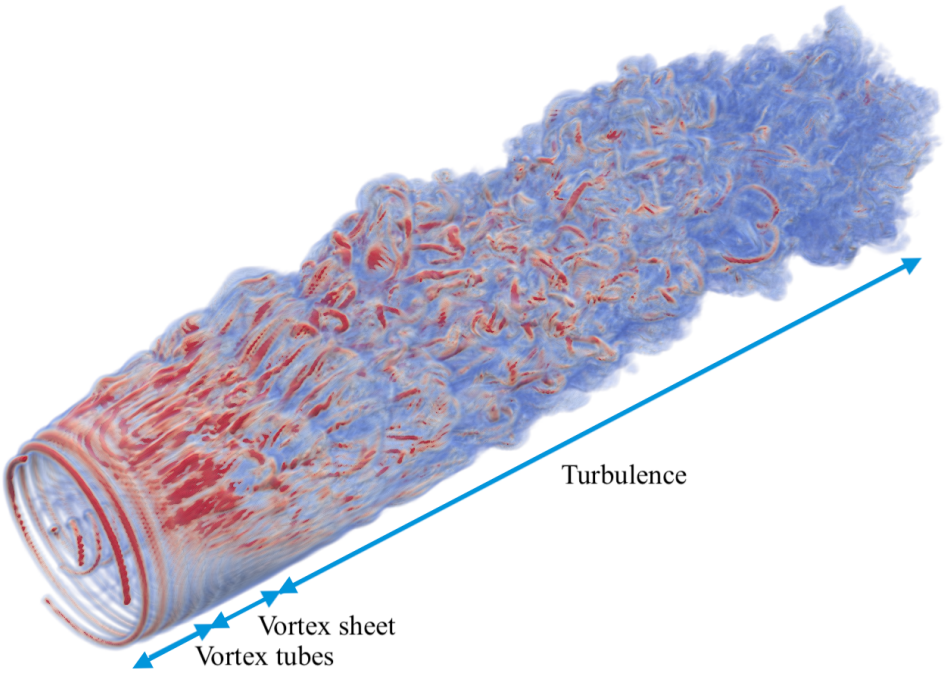

(b) VPM with added terms for the effect of shear on vorticity

Figure 2.4: Iso-contour of vorticity behind a wind turbine

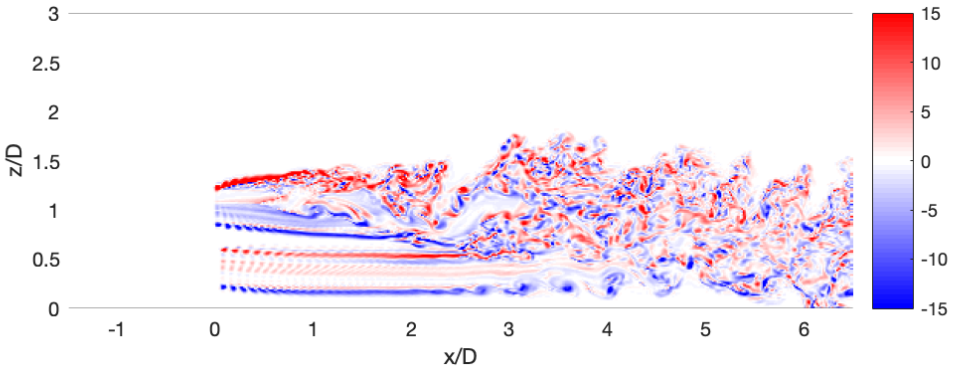

(a) VPM

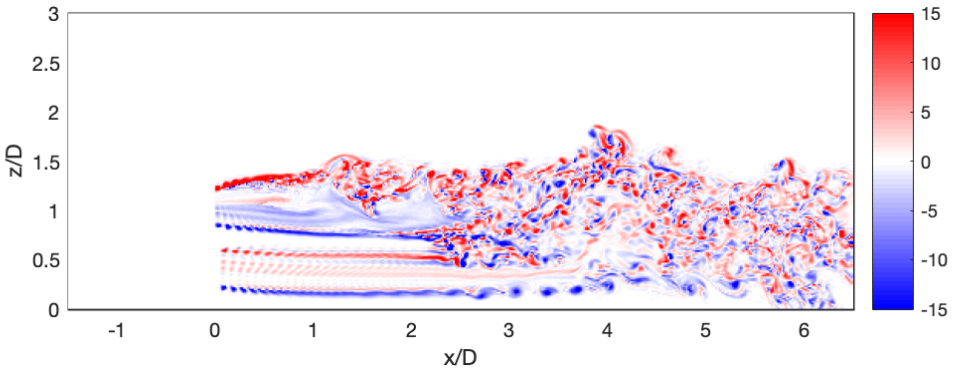

(b) VPM with shear effect modeling

Figure 2.5: Normalized y-vorticity $\frac{\omega_y D}{U_\infty}$ in direction in the vertical plane

However, in the case of the shear effect model, the top of the wake spreads a little higher. At approximately 1.5 diameters from the turbine, the flow has a recirculation region. At this point, the flow has already become highly turbulent and the vortex sheet has completely destabilized into turbulence. Although the wake does not have a general tendency to deviate upwards, it tends to leak upwards in certains regions, whereas this is not the case without shear effect modeling.

The bottom of the wake also undergoes a different behaviour than without shear modeling: The Kelvin-Helmoltz instabilities begin much closer to the blades, at around $x/D = 1.5$ versus $x/D = 2.5$ without shear effect modeling. As a consequence, the wake spreads less toward the bottom and maintains more of a parallel flow. These eddies are smaller and thus have less distance seperating them. At $x/D = 3$, they are much more defined than in the case without shear effect modeling and bottom of the wake begins to be deflected upwards. However,

the behaviours of the flows in the far wake are relatively similar, although the case without shear effect modeling has a pattern that appears at $x/D = 5$ that is reminiscent of Kelvin-Helmholtz instabilities.

The center of the the wake in the case of the model experiences a downwards inflexion towards $x/D = 2$. This seems to maintain the region without vorticity further along the streamwise direction than in the case without modeling. Indeed, the center of the wake mixes at $x/D = 2$ without the model and at $x/D = 2.5$ with it.

Streamwise velocity

Figures 2.6 and 2.7 depict the instantaneous and time-averaged streamwise velocities in the wake respectively. The behaviour at the top of the wake is different: since the wake with shear effect modeling contains less high velocity regions and more low velocity regions, the flow above the wake is accelerated. A parallel can be established between this behaviour and the concept of conservation of mass, where any deceleration of the flow has to be compensated by an acceleration on the same vertical plane.

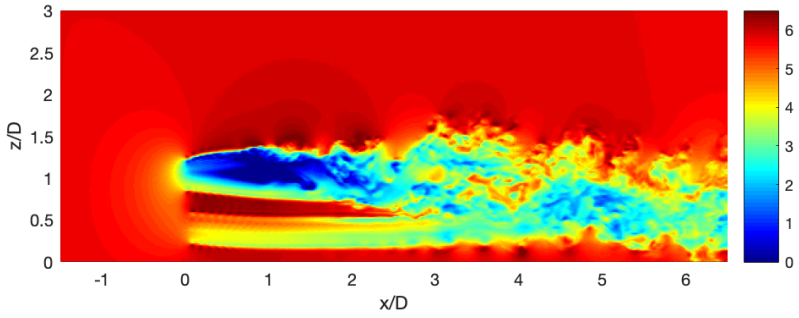

(a) VPM without shear effect modeling.

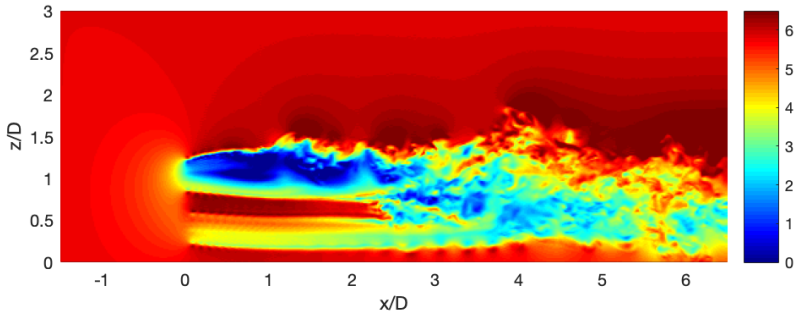

(b) VPM with shear effect modeling.

Figure 2.6: Instantaneous streamwise velocities for a linear wind velocity profile

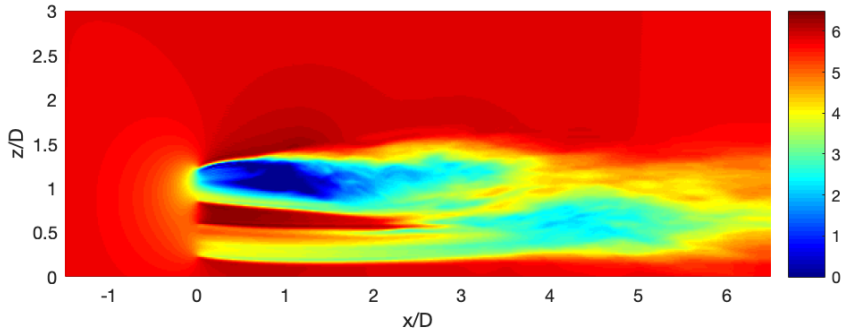

(a) VPM without shear effect modeling.

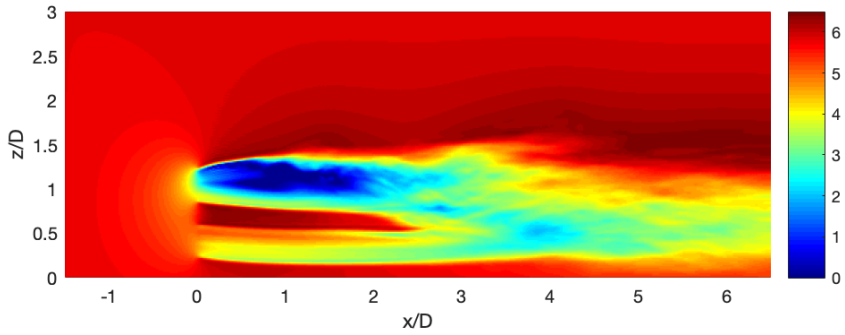

(b) VPM with shear effect modeling.

Figure 2.7: Time-averaged streamwise velocities for a linear wind velocity profile

The instantaneous snapshots reveal the tendancy of the modeled flow to leak upwards, like at $x/D = 4$. Despite the upwards deflection of the bottom of the wake at that point, the far wake with shear effect modeling is actually thinner and its center is lower. Without shear effect modeling, as the high velocity wake center disappears, it tends to leak upwards. With the model, this behaviour is less noticeable, as the increased vorticity homogenizes the low and high velocity regions.

Figure 2.8 depicts the time-averaged velocities of the cases with and without shear effect modeling in the y-z plane at different positions in the wake. Although not in the same plane, the trajectory of the blade tips has been outlined in black. These slices show that the acceleration of the flow outside of the wake is strictly restricted to being above the wake and not around it. At $x/D = 4$ in the case with shear effect modeling, the homogenization of low and high velocity regions is observable, as well as the upwards leakage.

In the far wake in the case without shear effect modeling, the flow is only influenced in the near the viscinity of the blade tips' outline. At $x/D = 2$, the only differences are above the flow. This highlights the fact that the model's effects are not instantaneous but rather develop along the wake, stacking in the middle/far wake while leaving the near wake almost untouched.

Surprisingly, the slices show strong asymmetricality with respect to the y-axis when the lifting lines correction is applied. To verify that this asymmetry isn't a consequence of simulation parameters, the same simulation was ran without the lifting lines correction and demonstrated a strictly axisymmetrical behaviour (refer to appendix A). It could be the result of a phase effect of the blade rotation with the data output time interval. However, this is most likely the result of too short of a time window for the gathered statistics, despite it covering 6 revolutions.

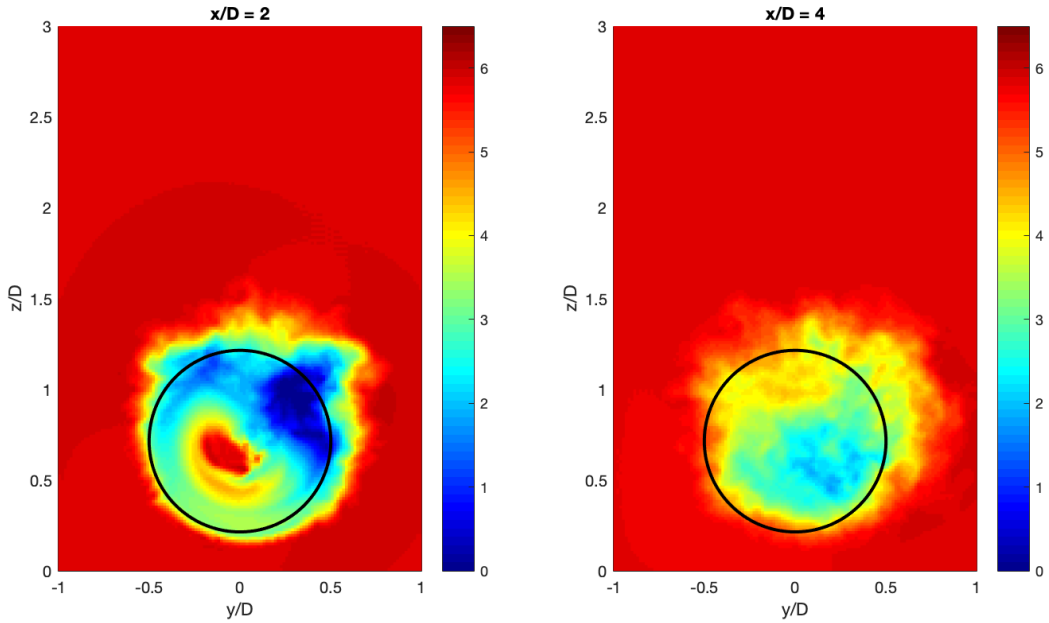

(a) VPM without shear effect modeling.

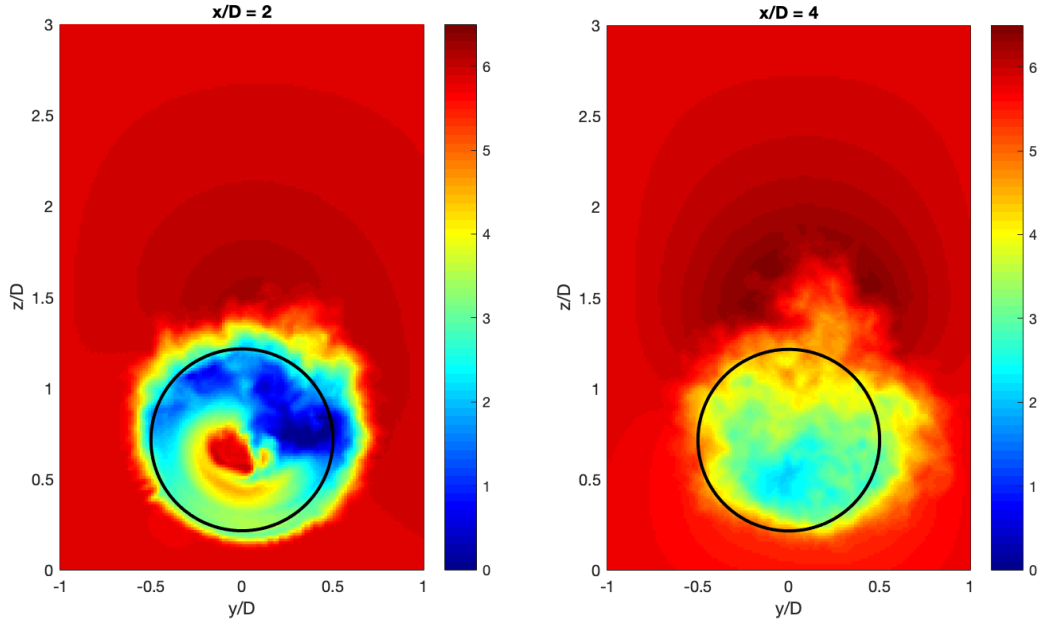

(b) VPM with shear effect modeling.

Figure 2.8: Time-averaged streamwise velocities in the y-z plane.

Figure 2.9 shows the time-averaged velocity deficits in the wake at various positions. Expectedly, at $x/D = -1$ amd $x/D = 0$, the velocity deficit profiles are identical. At $x/D = 1$, the behaviour of the top of the wake starts to change. The low velocity region created by the blades is slightly deflected upwards. However, the bottom of the wake remains identical. At $x/D = 2$, the bottom of the wake is still identical whereas the top spreads: at $z/R = 1.5$, the velocity deficit of the model is 0, while the case without model is 0.2. The model sees a greater velocity deficit at the top of the wake and a larger high velocity wake center.

From that point onwards, the flow has multiple caracteristics: the model tends to slow down the bottom of the wake, although the values of the two cases at $z = 0$ are very close. The top of the wake is faster and the center of the wake of the model is lower.

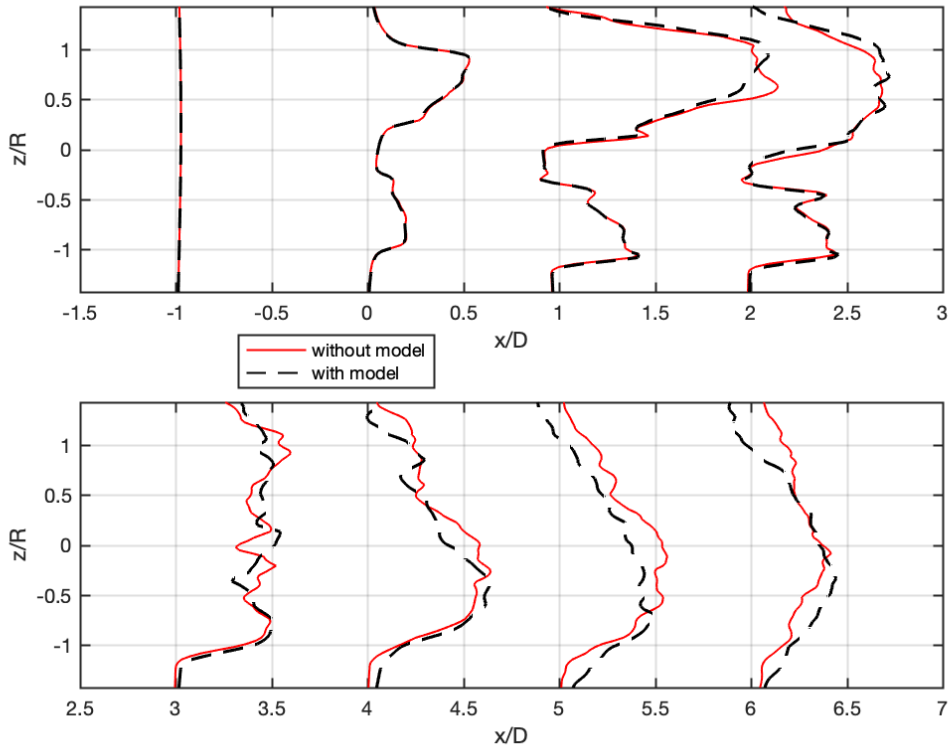

Figure 2.9: Time averaged velocity deficit $\frac{U_\infty - u_x}{U_\infty}$ with and without shear effect modeling.

2.2 Power law profile

In this section, the effects of a power law velocity profile upstream of the turbine are investigated. The previous section briefly explained how the linear profile was computed from a least-squares linear regression applied to this non-linear profile. The power law profile obeys the following equation:

$$\frac{U}{u_h} = \left(\frac{z}{z_h}\right)^{\alpha} \tag{2.3}$$

where $u_h = 5.79$, $z_h = 90$ and $\alpha = 1/9$. The simulations will now be carried out with this non-linear profile for two main purposes:

- Making use of the second-order derivative $\frac{\partial^2 U}{\partial z^2}(z)$ that appears in the Navier-Stokes equation 1.22 used for shear effect modeling.
- Applying the model to a more realistic velocity profile, as can be found in nature.

The main hypothesis of this section is that the second-derivative term of the shear effect model is predominant in its effects on the flow. Indeed, by simplying the problem to a 2-D case, a better understanding of which part of the model is predominant in its effects on the flow can grasped. Let's consider a two-dimensional case: The same system of axes is used, but the flow is two-dimensional in the x-z plane. This implies that: $v = 0$, $\omega_x = 0$, $\omega_z = 0$ and $\frac{d}{dy} = 0$. The system of equations 1.22 becomes:

$$\frac{D}{Dt}\omega_y = -\frac{d\Omega}{dz}w = -\frac{d^2U}{dz^2}(z)w \tag{2.4}$$

In the two-dimensional case, only one term of the system of equations 1.22 remains: the product of the second derivative of the velocity profile with the z-velocity of the flow. Since the wind velocity profile is exactly the same in the 2-D case and the 3-D case, it can be expected that the term present in the 2-D case will have the most influence on the vorticity and wake of the wind turbine in the 3-D case.

This hypothesis will be tested by running simulations with what will be called the partial shear effect model: a version of the shear effect model with all terms but the second derivative product turned off. The viscosity term $\nu\nabla^2\boldsymbol{\omega}$ is very small in the context of this thesis and the SGS term acts as part of a numerical model. For the sake of clarity, these terms are not displayed in the equations of the following sections, despite being present in the VPM code:

$$\frac{D}{Dt}\omega_x = \frac{\partial u}{\partial x}\omega_x + \frac{\partial u}{\partial y}\omega_y + \frac{\partial u}{\partial z}\omega_z \tag{2.5}$$

$$\frac{D}{Dt}\omega_y = \frac{\partial v}{\partial x}\omega_x + \frac{\partial v}{\partial y}\omega_y + \frac{\partial v}{\partial z}\omega_z - \frac{\partial^2 U}{\partial z^2}w \tag{2.6}$$

$$\frac{D}{Dt}\omega_z = \frac{\partial w}{\partial x}\omega_x + \frac{\partial w}{\partial y}\omega_y + \frac{\partial w}{\partial z}\omega_z \tag{2.7}$$

The term colored in red will be referred to as the 2-D term of the model, while the other omitted terms present in the complete model will be referred to as the 3-D terms of the model.

2.2.1 Velocity profile masking

The exponential character of the power law implies that the velocity is zero at $z = 0$. However, velocity is only relevant in the computation of the lifting lines method, whereas its first and second derivatives are present in every term added to the NS equations for shear effect modeling. The exponential caracter of the power law generates asymptotic behaviour at $z = 0$ for the derivatives, creating unstable behaviour once vorticity approaches this zone. The derivatives $\frac{dU}{dz}$ and $\frac{d^2U}{dz^2}$ approach infinity and negative infinity respectively as z approaches zero. To prevent vorticity from exploding in this zone, a mask is applied to bring the derivatives back to zero very close to the interface.

The filter applied is the following:

$$G(z) = exp(-\frac{(z - n\Delta z)^2}{2\sigma(\Delta z)^2}) \tag{2.8}$$

where σ and n are adimensional coefficients that adjust the steepness of the mask and the number of grid points away from $z = 0$ where the mask is applied respectively. These coefficients are set at $\sigma = 4$ and $n = 5$, corresponding to the tamest mask that can be applied and still prevent accumulation of vorticity near $z = 0$. The first and second derivatives thus become:

$$\frac{dU^*}{dz}(z) = G(z) \cdot U(z) \tag{2.9}$$

$$\frac{d^2U^*}{dz^2}(z) = \frac{d^2U}{dz^2}(z) \cdot G(z) + \frac{dU}{dz}(z) \cdot \frac{dG}{dz}(z) \tag{2.10}$$

The behaviour of the first and second derivatives with and without the applied mask can be observed in figure 2.10.

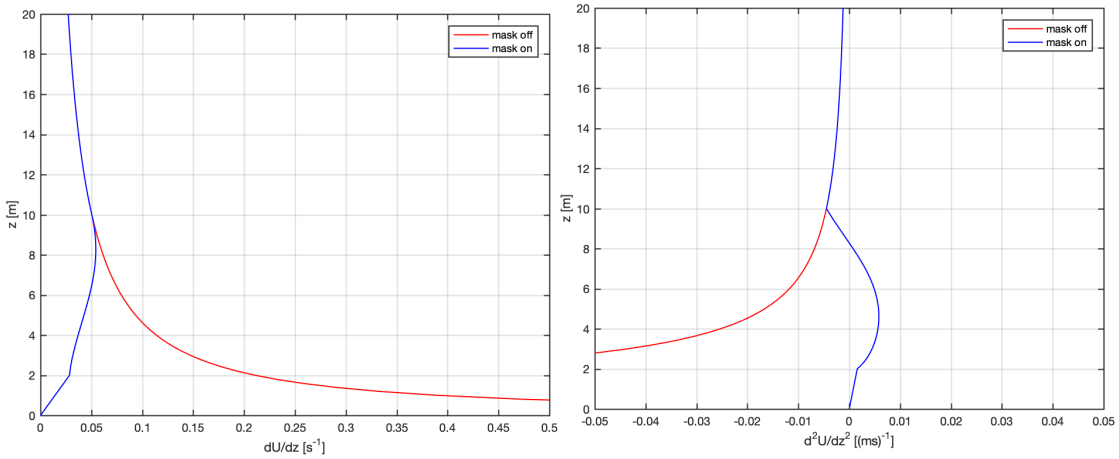

Figure 2.10: Masks applied to the first and second derivatives of the velocity profile.

Both masks generate local maxima between $z = 5$ and $z = 10$. Furthermore, when deriving the first derivative with mask to obtain the second, it creates a region of positive values between $z = 0$ and $z = 8$, despite the rest of the domain containing strictly negative values. Although necessary to perform the simulations, this mask will prove to be a consequent source of inaccuracy.

2.2.2 Boundary conditions

In order to replicate a more physically accurate scenario, the simulations are no longer performed with unbounded boundary conditions. Ideally, simulations would be performed with a no-slip condition at the interface $z = 0$. However, in the context of vortex methods, one of the main difficulties resides in enforcing this condition at the wall.[15] The 3-D Navier-Stokes equations in vorticity-velocity formulation will thus be solved with a No-Through Flow (NTF) condition at the wall. Mathematically, this corresponds to $\mathbf{u} \cdot \mathbf{n} = 0$ at the wall. The NTF condition thus only restricts normal velocity to zero, without directly affecting tangential velocity.

Applying the NTF condition in the z-plane implies applying it to both bottom and top interfaces. However, in the context of these simulations, a top NTF condition is not required, but can be used to model the top of a boundary layer, where $\frac{du_x}{dz} = 0$. For this reason, the domain size has to mimic the thickness of the atmospheric boundary layer modeled by the power law. However, since the turbine is already so close to the ground and far from the upper boundary, the domain size was arbitrarily increased in the z-direction, from $z_{max} = 378$ to $z_{max} = 756$ (see

figure 2.11). A more correct way of increasing the domain height would have been to increase it to whatever the size of the atmospheric boundary layer the power law is modeling. However, the approximation was deemed adequate as the effects of a no-through flow condition on the general flow were deemed negligeable when so far from the hub. For the sake of clarity, the figures produced in the following sections only display data in the domain $z = [0, 378]$, but were computed with the increased domain $z = [0, 756]$.

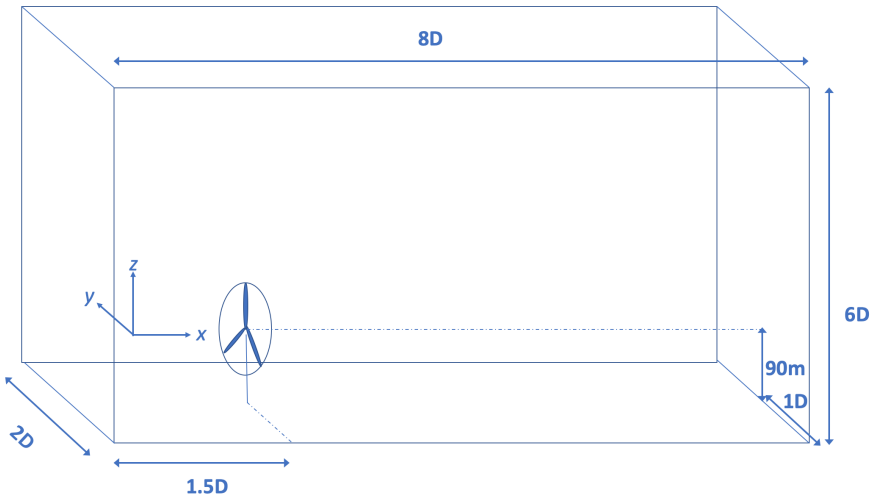

Figure 2.11: Computational setup for the power law shear wind profile.

Figure 2.12 displays the effects of these boundary conditions on the VPM simulations without shear effect modeling. At the blades, the flow with no-through flow boundary conditions is already faster. As the wake develops, the difference in velocities of the flows keeps increasing. This can be seen as a consequence of conservation of mass: since the top and the bottom boundary conditions are NTF, the flow can be compared to a channel flow. The flow can no longer deviate below $z = 0$, the sectional area in NTF is smaller than in unbounded conditions. Since the mass flow rate remains constant, the flow reacts by deviating upwards (as it no longer has room to "spread" below) and accelerating. The deviation of the flow can be observed by noticing that the center of the wake (the local minimum of the velocity deficit) increases in altitude.

A byproduct of this acceleration of the flow is the increased turbulence that in turn accelerates the mixing of the flow. This can be observed 4 diameters behind the wake, where the high velocity region in the center of the wake disappears for the NTF case but not yet the unbounded one. In the far wake, the differences between the flows are less distinguishable. In the case of NTF boundary conditions, the velocity close to $z = 0$ is smaller.

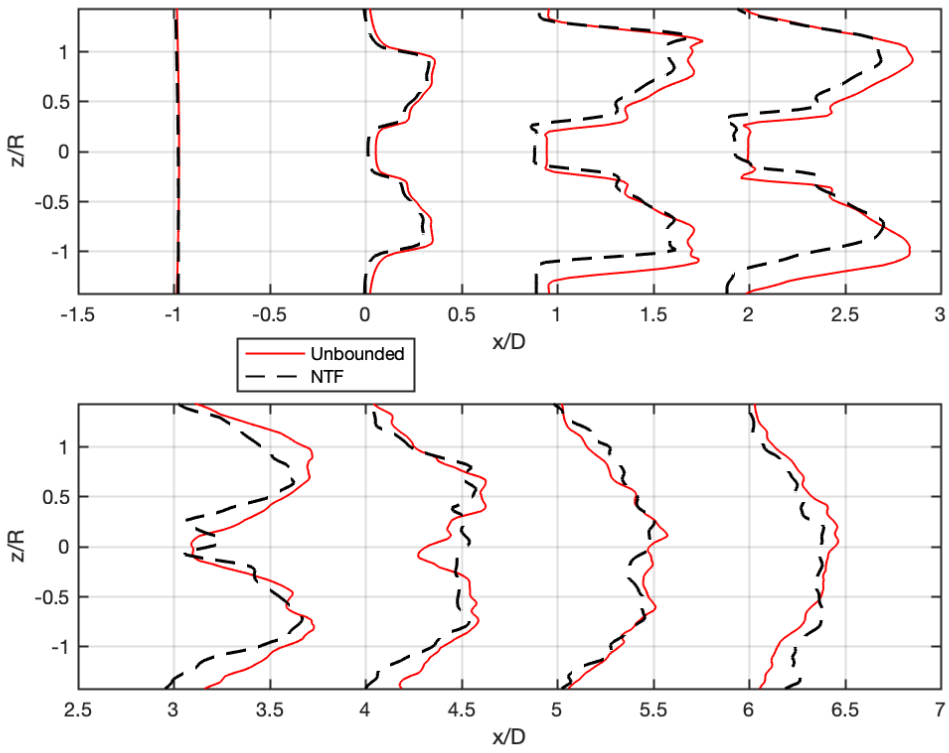

Figure 2.12: Time averaged velocity deficit $\frac{U_\infty - u_x}{U_\infty}$ without shear effect modeling for unbounded and NTF boundary conditions.

2.2.3 Behaviour of the model

Figure 2.13 depicts the normalized instantaneous y-vorticities for the case without shear effect modeling, with the previously established partial shear effect model and finally its complete version. The deflection of the wake due to the NTF condition is noticeable in the deflection of the center of the wake of the case without shear effect modeling. It is important to distinguish what is caused by the NTF condition from what is caused by the power law profile.

The differences in the wake behaviours of the partial and complete shear effect models are small. Predictibly, the main differences occur in the behaviour of the bottom of the wake. When the 3-D terms are present in the complete shear effect model, the Kelvin-Helmholtz instabilities develop closer to the turbine and transition faster into turbulence than in the case of the partial model.

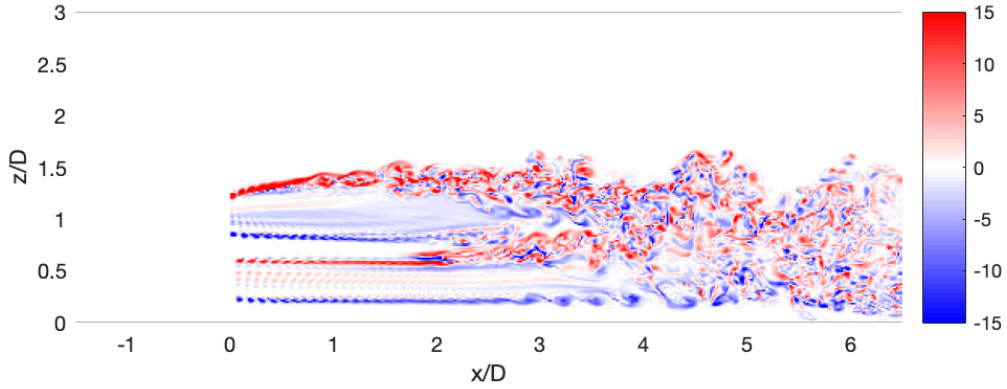

(a) VPM without shear effect modeling.

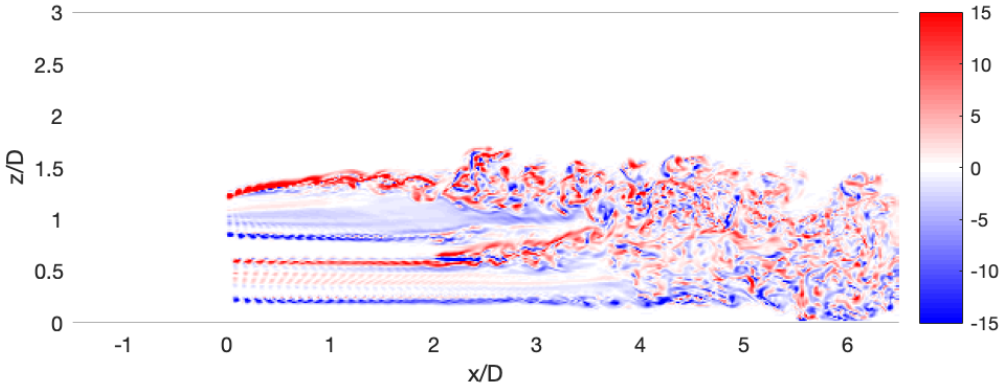

(b) VPM with partial shear effect modeling.

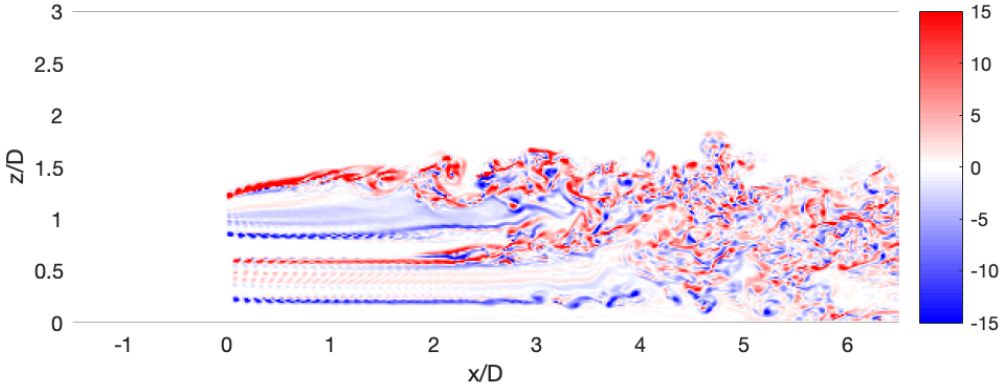

(c) VPM with complete shear effect modeling

Figure 2.13: Normalized y-vorticity $\frac{\omega_y D}{U_\infty}$ in the vertical plane

Figure 2.14 depicts the time-averaged streamwise velocities of the different cases. It can be observed that the differences between the cases with partial shear effect modeling and without modeling are much smaller than the effect created by the lifting lines correction. This is a first indication that the effect of the model compared to the effect of the corrected lifting lines method is small. In the case of the complete shear model, the flow has a low-velocity region close to $z = 0$, approximately five diameters from the turbine. The streamwise velocity falls to almost zero. This can be justified by the fact that all 3-D terms are products of $\frac{dU}{dz}$, which, despite the applied mask, has much greater values in this region. The 3-D terms thus cause the far wake to be deflected downwards. This low-velocity region is compensated by a high velocity region above the wake, thus conserving mass flow rate.

Figure 2.15 depicts the time-average velocity deficits of the different cases. In the near-wake, the partial and complete shear effect model cases are practically identical. At $x/D = 2$, the effects of the 3-D terms start to appear: the increased turbulence slows both the top and the bottom of the wake of the complete model case down. The velocity deficits quantify the previously explained behaviour of the influence of the 3-D terms near $z = 0$. As the flow evolves away from the turbine, the complete model sees a decrease in streamwise velocity close to the boundary with respect to the partial model. The velocity deficit plots highlight how little influence the 2-D term has on the flow. In fact, the velocity deficits of the cases with partial shear effect modeling and no modeling are almost identical. Small differences appear from $x/D = 2$ onwards, especially at the local minima and maxima. However, the behaviour generally remains very similar.

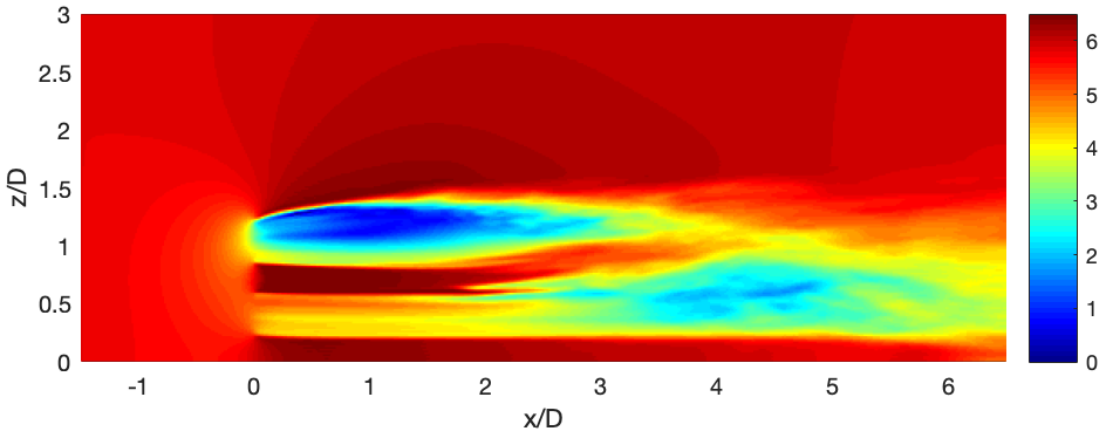

(a) Time-averaged streamwise velocity without shear effect modeling.

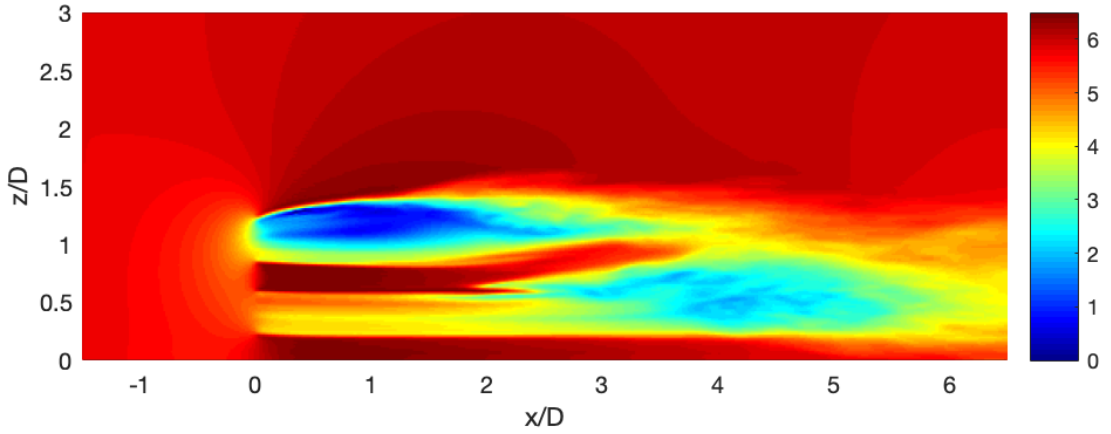

(b) Time-averaged streamwise velocity with partial shear effect modeling.

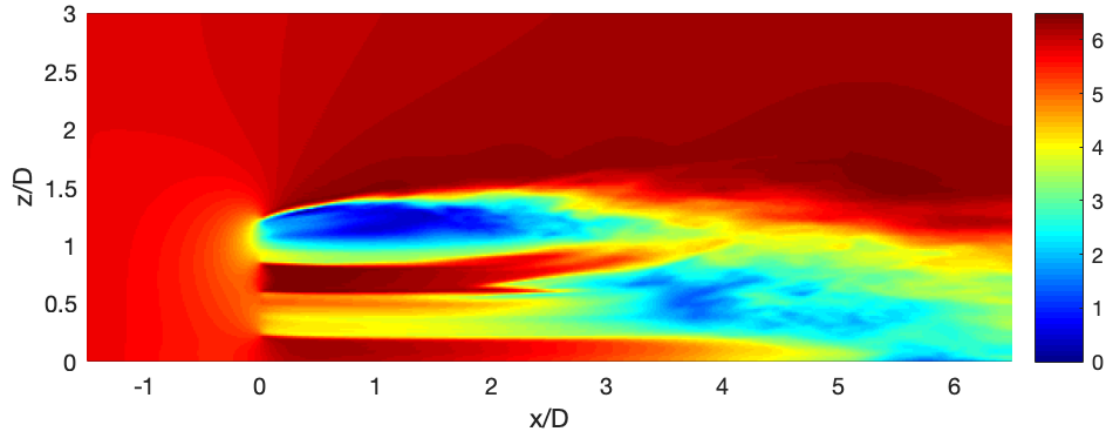

(c) Time-averaged streamwise velocity with complete shear effect modeling

Figure 2.14: Isocontours of mean velocities

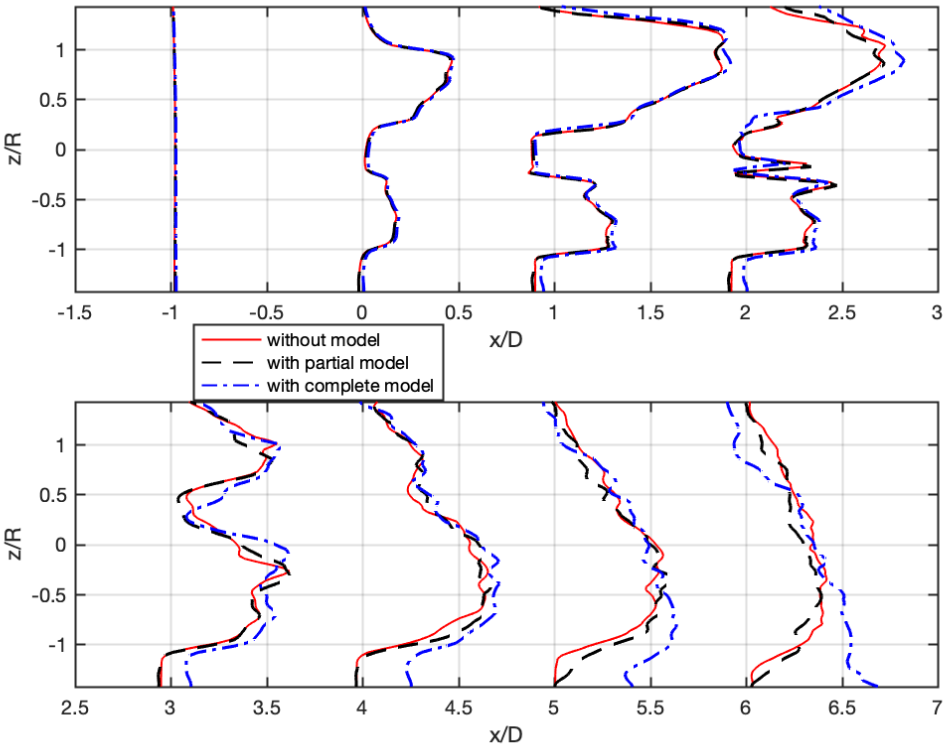

Figure 2.15: Time averaged velocity deficit $\frac{U_\infty - u_x}{U_\infty}$ without shear effect modeling, with partial shear effect modeling and complete shear effect modeling.

2.3 Conclusion

The main assumption of the shear effect model resides in the lack of interaction between the vorticity created by the turbine and the vorticity that is a consequence of the velocity profile. The aim of this chapter was to provide a preliminary understanding of how the model behaves with respect to a simulation without shear effect modeling, and thus understand where the model influences the flow the most.

In section 2.1, due to the chosen linear profile, the shear effect model only relies on its 3-D terms to act upon the vorticity in the wake. Although the shear effect model has very little impact in the near wake, it is responsible for creating more vorticity and thus turbulence in areas where the latter is already present. This phenomenon is witnessable on the top and bottom extremities of the wake, accelerating its transition into a turbulent state. In the far wake, the model creates a faster flow above hub height and a slower one below. Although the velocity of the particles entering the domain remain uniform, the lifting lines method acts upon the velocity profile given as input, thus shedding more vorticity when the blades are higher than the hub and less when the blades are lower. Since this vorticity is not compensated particles whose velocities are those of the profile, the blades create a distinguishable low velocity region at the top of the wake and a high velocity region at the bottom. This has the effect of deflecting the center of the wake downwards, a behaviour that can seem counter-intuitive. Chapter 3 will clarify if the opposite behaviour occurs in simulations where the velocity field of the particles corresponds to that of the velocity profile given as input.

Section 2.1.3 sought to split and analyze the model based on the hypothesis that the only term present in the derivation of the model in a 2-D case has a predominant effect on the flow. Two variants of the model were thus run: one with all terms activated and one with only the term appearing in the 2-D case activated. This section attempted to model a more physical scenario where the boundary conditions were closer to that of nature: a power law velocity profile making the 2-D term non-null and a NTF condition at the ground and the top of the boundary layer.

It was observed that the 2-D term is responsible for most of the different behaviour and deflection of the wake, although the NTF condition played its role in the latter. The 3-D terms have a more significant close to the ground impact in the case of the power-law profile due to its high values its first derivative in this region. Their effect was noticeable through the faster developping Kelvin-Helmholtz instabilities at the bottom of the wake and the low velocity region close to the ground in the far wake. In fact, without the 3-D terms, the velocity deficit profiles

of the partial model and the case without shear effect modeling are almost identical at 6+ diameters from the turbine. This hints that the 3-D terms are necessary for the model to accurately represent the real-life scenario, as they create a particle field with a velocity profile that corresponds more to that of the one modeled.

Chapter 3

Model Accuracy

The previous chapter carried out an investigation on how the model affects the flow and in which ways the different terms react to the wind profile given as input. Whereas the shear effect model uses a uniform particle velocity field and attempts to model only the effects of the wind velocity profile on vorticity, this chapter uses simulations performed with the velocity profile applied directly onto the particles entering the computational domain in order to establish the model's accuracy by comparison.

Contents

3.1 Power law profile

In this section, "VPM with exact shear modeling" refers to the case where the full interaction between the shear vorticity derived from the shear velocity profile $\boldsymbol{\Omega} = \frac{dU}{dz}(z)\mathbf{e}_y$ and the additional vorticity $\boldsymbol{\omega}$ is taken into account. The vorticity of the flow is thus considered to be $\boldsymbol{\omega}_{tot} = \boldsymbol{\omega} + \boldsymbol{\Omega}$, and the NS equations take into account the global vorticity without the use of the shear effect model:

$$\frac{D\boldsymbol{\omega}_{tot}}{Dt} = (\boldsymbol{\omega}_{tot} \cdot \nabla)\mathbf{u} + \nu\nabla^2\boldsymbol{\omega}_{tot} + \nabla \cdot \mathbf{T}^M \tag{3.1}$$

To perform this, the shear vorticity $\boldsymbol{\Omega}$ is interpolated onto the particles entering the domain. The same mask as the previous chapter is used near $z = 0$ to prevent undesired accumulation of vorticity due to the asymptotic behaviour of the power law's derivatives in this region. Contrarily to the model, the shear vorticity of the exact case acts at the turbine blades, whereas the model only acts three meters behind the latter to prevent undesired interaction of vorticity with the lifting lines method. The shear effect model and exact model thus do not act on the same domain.

3.1.1 Results and discussion

Figure 3.1 depicts instantaneous vorticity slices in the vertical plane. In the case of exact shear modeling, the shear vorticity profile is directly interpolated onto the particles upon entry of the computational domain. Although its values are too low for the chosen colormapping to represent them at hub height, greater values of vorticity are noticeable close to the ground. This highlights the difference in magnitude of the shear vorticity and the vorticity generated by the turbine, which is predictably greater.

Although the mask is not observable ($z \leq 10$m), it represents a source of inaccuracy. The effect of the shear vorticity profile close to the ground is noticeable as the bottom of the wake sees Kelvin-Helmholtz instabilities develop closer to the turbine. The flow then rapidly transitions into a turbulent state.

Compared to the exact reference case, the model generates more vorticity above hub height and less below, due to the applied lifting lines correction. This is noticeable as the vortex tubes of the model transition earlier ($x/D = 1/4$ vs. $x/D = 1$) into a vortex sheet above hub height, and later ($x/D = 2$ vs. $x/D = 0.5$) below.

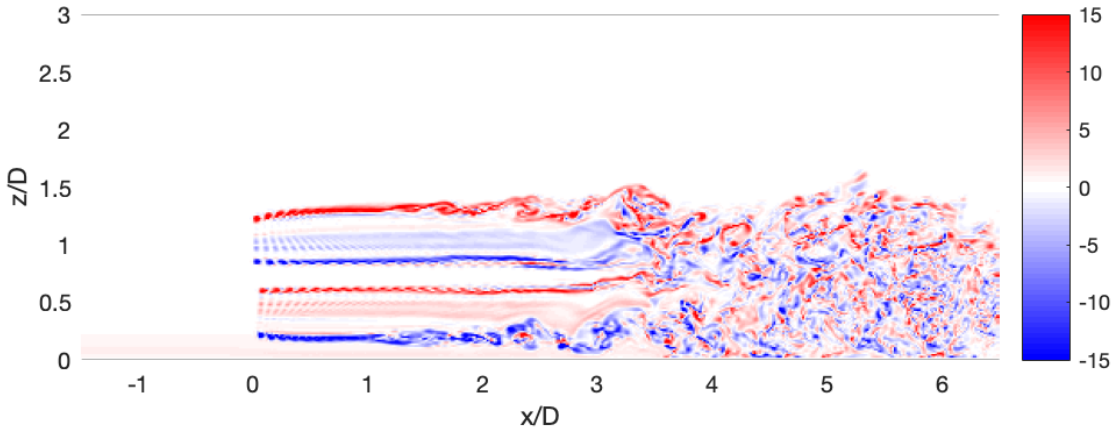

(a) VPM with exact shear modeling.

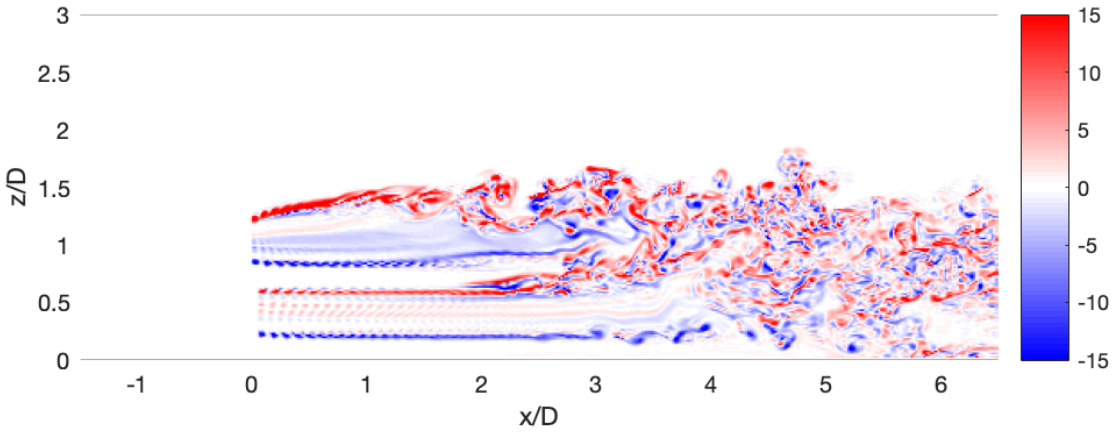

(b) VPM with complete shear effect modeling

Figure 3.1: Instantaneous normalized y-vorticity for a power law profile.

Contrarily to all the simulations ran by the shear effect model until this point, the effect of the shear vorticity is very subtle when ran with the exact model. In fact, there is almost no deviation in the wake, except towards $x/D = 3$. It is safe to say that the behaviour of vorticity in the wake of the exact case is closer to the one without a shear velocity profile than to the model. However, when the NTF boundary condition was the sole actor on the flow, the wake saw a slight deviation upwards. The shear effect model seems to compensate this behaviour, indicating that shear vorticity deflects the wake downwards.

The colormapping of the figures also highlights the fact that the shear effect model tends to generate vorticity of greater magnitude, as can be observed at the top of the vortex sheet.

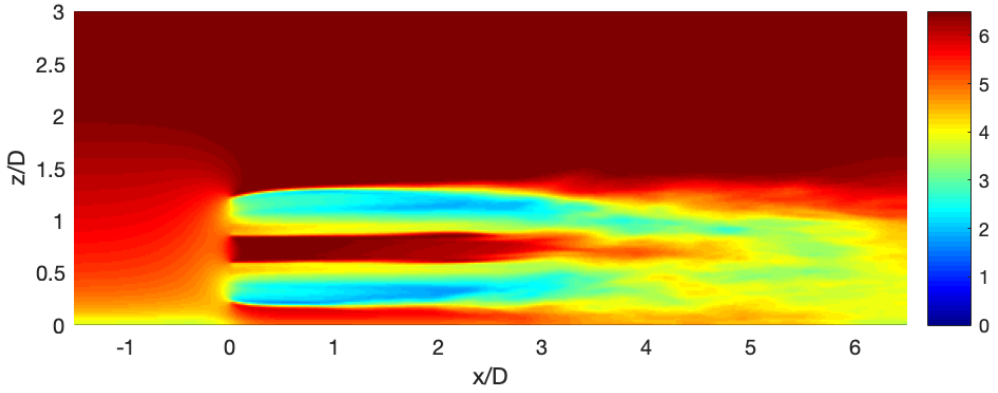

(a) VPM with exact shear modeling.

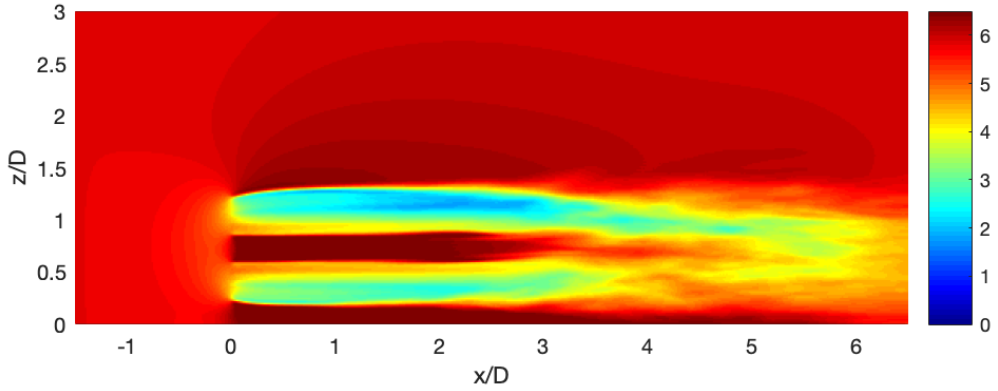

(b) VPM with exact shear modeling and applied velocity field correction.

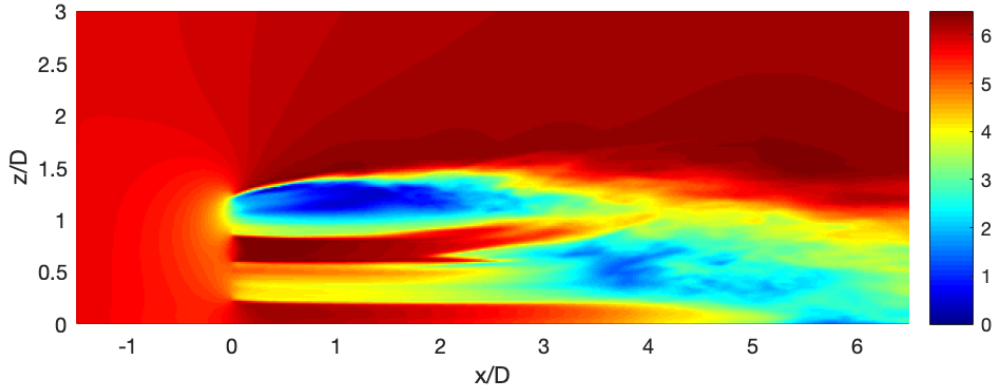

(c) VPM with complete shear effect modeling.

Figure 3.2: Time averaged streamwise velocity for a power law profile.

Figure 3.2 depicts the time-averaged streamwise velocities of the flows in their different cases. These time-averaged statistics showcase the lack of accuracy of the model. Figures (a) and (c) do not bear any ressemblance to each other. In order to offer a more relevant comparison, the time-averaged velocity field of the exact shear model is also represented with a correction applied to it : the velocity field upstream of the turbine is subtracted from the particles over the entirety of the domain, then the uniform upstream velocity of the particles of the shear effect model is added back. This makes it so that the particle velocities upstream of the turbine are equivalent to the ones of the model. Although this does not make the model and the exact simulations physically equivalent, it provides an idea of the orders of the magnitude the shear effect model should seek to replicate. This doesn't modify the shape of the wake but accentuates where the low and high velocity regions should be.

The positions of the regions of low velocity of the far wake of the uncorrected exact shear model are relatively accurate, yet the values are not coherent. Since the model creates a generally more turbulent flow, the values of its low velocity regions are lower. Generally speaking, the wake is slower than in the exact shear model, except at the bottom of the wake near the turbine.

Despite the inaccuracy of the mask applied close to the ground, the high velocity region beneath the wake is mimicked with relative accuracy. At this point, it is clear that the shear effect model does not accurately model the velocity field of the exact model. However, when applying the correction to the velocity field, the same regions of high and low velocity at the bottom and top of the wake appear, although their values are not comparable. The same strip of high velocity is found right under hub height from $x/D = 0$ to $x/D = 2$.

One of the most apparent discrepancies between the shear effect model and the exact model can be found in the deflection of the high velocity wake center of the shear effect model that begins at $x/D = 2$.

The velocity deficit plots in figure 3.3 also contain information about both the corrected and uncorrected velocity fields of the exact shear model's simulations. In the case without correction, the velocity deficit highlights the shear effect model's opposite behaviour to the exact case. Whereas the exact case predictibly creates a low velocity region at the bottom of the wake and a higher velocity region at the top for $x/D = 0$, the model almost creates a opposite symmetrical behaviour to the exact case around the hub height. Indeed, the velocity deficit matches in this region due to the lack of interaction with the blades, and thus lack of vorticity. The discrepancies above and below the hub are a consequence of the uniform velocity

field of the upstream particles being acted upon by the lifting lines method that perceives the wind velocity profile. The velocity of the particles below the hub is thus greater with shear effect modeling than in the exact case, since the lifting lines method sheds less vorticity in this region. The opposite behaviour occurs above hub height.

The shear effect model does however accurately represent the general behaviour of the wake in $x/D = 1$: the local minima and maxima share the same altitude, albeit not the correct values. The exact shear model sees its velocity of its top and bottom regions of the wake equalize, while the low velocity region of the shear effect model keeps decreasing in magnitude. As a consequence, the difference in velocities of the top and bottom regions is large.

At $x/D = 2$, the discrepancies between the two wakes decrease, but the position of the local minima and maxima of the bottom of the wake of the shear effect no longer mimics that of the exact case. From this point onwards, the wake begins deviating upwards, thus increasing the inaccuracy of the shear effect model. Finally, the shear effect model gains in accuracy in the far wake, especially from the hub height and upwards. In the region close to the ground, the flow of the complete model is too slow while that of the partial model is too fast.

The figure with correction more accurately represents the flow of the exact case. Although the correction helps the region below and above the to be more accurate, it is not enough to compense the high velocity deficit at the top of the wake and low velocity deficit at the bottom. Although closer to the values of the shear effect model, the correction overcompensates the low velocity close to the ground, resulting in a velocity faster than the one at hub height. The partial shear effect model is more accurate to the corrected reference case at $x/D = 6$, although it is just a coincidence.

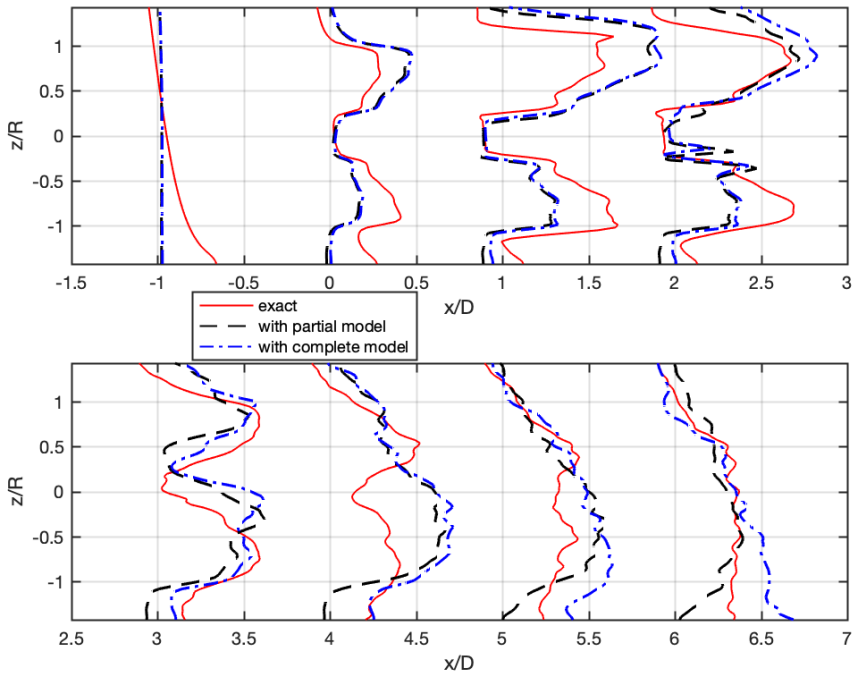

(a) Without velocity field correction.

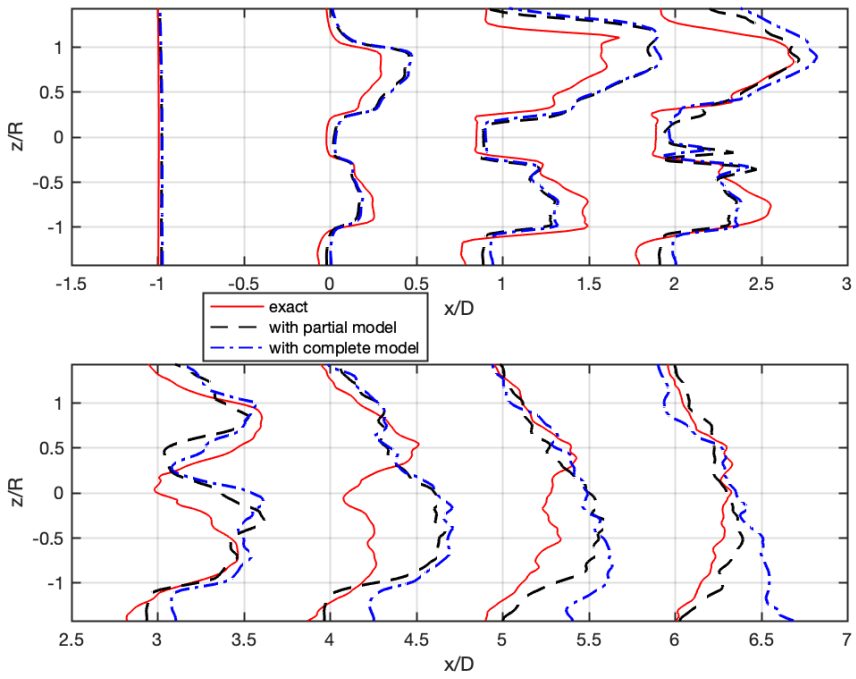

(b) With velocity field correction applied to exact VPM case.

Figure 3.3: Time averaged velocity deficit profiles $\frac{U_\infty - u_x}{U_\infty}$ with exact shear, partial shear effect and complete shear effect modeling for a power law profile.

3.2 Coles profile with BigFlow

In this section, the VPM shear effect model is compared to a simulation run with *BigFlow* with full interaction of the shear vorticity with the additional vorticity. The wind turbine used as reference is still the NREL-5MW offshore wind turbine, but this time running at 10.3 RPM with an upstream velocity of 9 m/s, which represents the maximum of the power curve of this turbine.

Similarly to VPM, *BigFlow* computes the flow using LES with an in-house developped 4th order finite difference to solve the NS equations supplemented by a subgrid scale model. However, the blades are modeled using an actuator line model instead of the lifting lines method. Another important difference between the VPM and *BigFlow* codes resides in the use of wall modeling for the latter. The velocity near the wall is obtained as

$$\frac{1}{u_\tau} = \frac{1}{\kappa|\langle \mathbf{u} \rangle|} \tag{3.2}$$

with $\kappa = 0.38$ the von Karman constant.

3.2.1 Velocity profile

The two simulations are run with a more physically accurate upstream velocity profile: the Coles composite profile that reads:

$$\frac{\bar{u}}{\bar{u_\tau}} = \frac{1}{\kappa} \log(\frac{z}{z_0}) + G(\eta) \tag{3.3}$$

where $\eta = z/\delta$, $\kappa = 0.38$, z_0 is set to 2.8mm and u_τ to 0.33m/s to recover the speed of 9m/s at the hub. $\delta = 1008$ is the height of the boundary layer.

$$G(\eta) = D(3(\alpha\eta)^2 - 2(\alpha\eta)^3) \tag{3.4}$$

where D=2.70 for a turbulent boundary layer, and α is set so that $\frac{du}{dz} = 0$ when $\eta = \frac{z}{\delta} = 1$. The no-through flow boundary condition theoretically should be applied at $z = 1008$ in order to reproduce the behaviour of the end of the boundary layer. Since the boundary of the domain is already much higher than the hub height, it was decided to keep the domain height at $z = 756$ to cut back on computational costs. Refer to appendix C for plots of the velocity profile and its first and second derivatives.

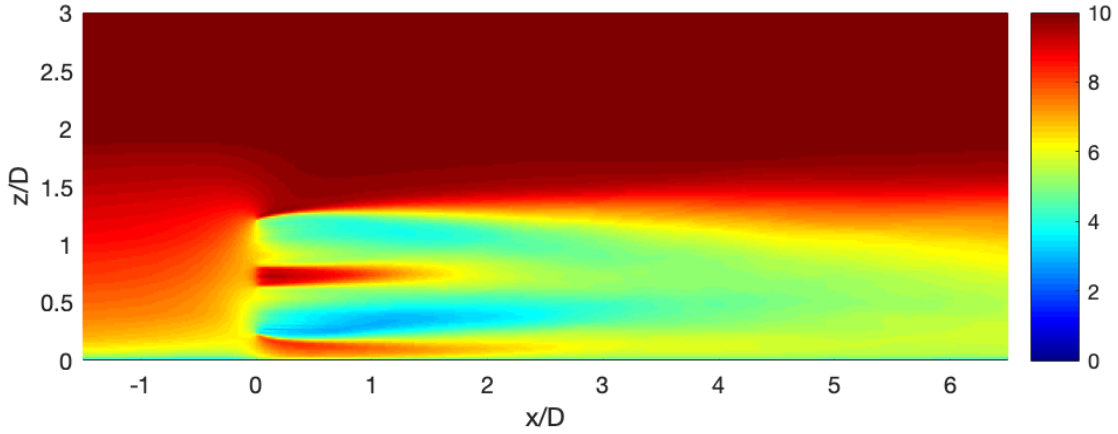

(a) *BigFlow* with exact shear modeling.

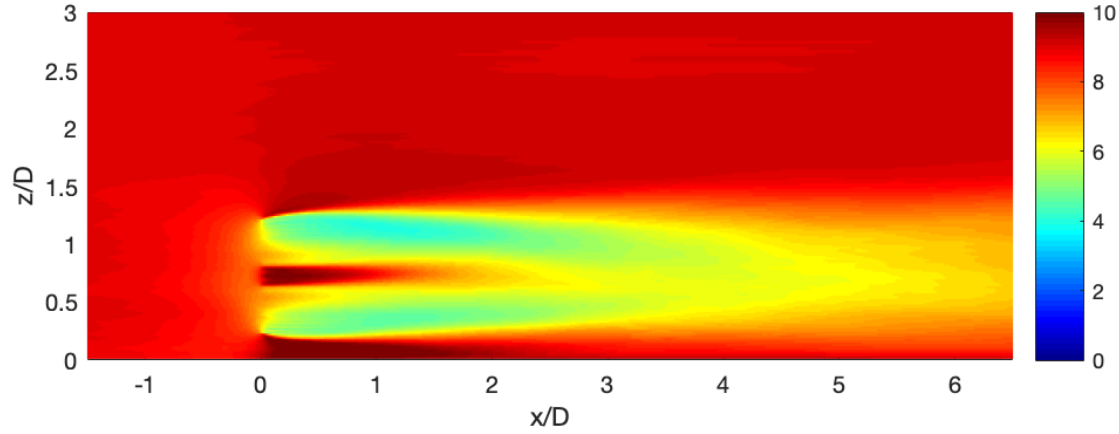

(b) *BigFlow* with exact shear modeling and applied velocity field correction.

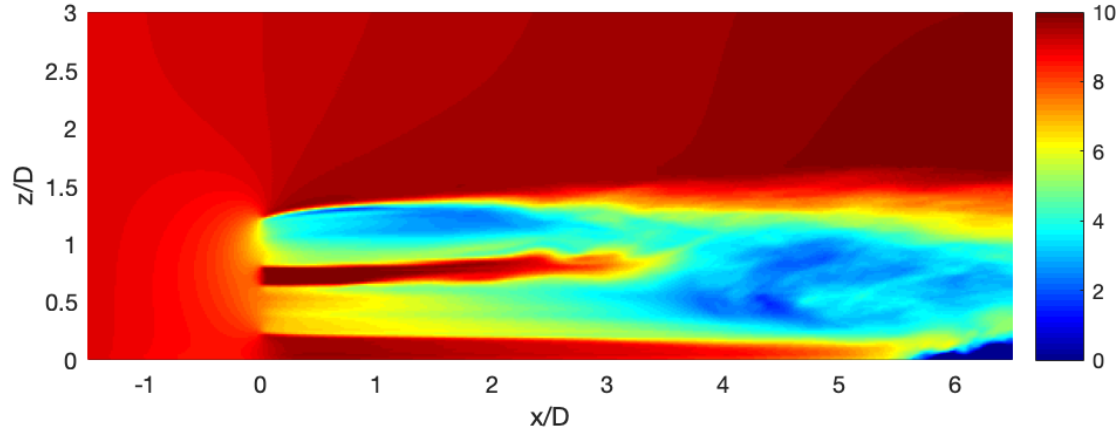

(c) VPM with complete shear effect modeling.

Figure 3.4: Time averaged streamwise velocity for an ABL profile.

3.2.2 Results and discussion

Figure 3.4 depicts the time-averaged streamwise velocity. Expectedly, the flow behaves similarly to the power law profile case. The atmospheric boundary layer model is steeper and thus sees greater values of its first derivative. Since the 2-D term has a greater impact near the ground and depends on the vertical velocity component, the model fails to correctly model the flow near the ground in the near wake. Once the wake spreads to the ground, near $x/D = 4$, the model quickly develops a comparatively larger low velocity region relative to the power law case.

Figures 3.5 and 3.6 represent the time-averaged velocity deficits of the two cases with and without the velocity field correction. At the blades, the model accurately represents the top half of the wake, although this could be the result of almost negligeable first and second derivatives at that height. It could also be a consequence of the actuator line model used with *BigFlow*. However, the model sees a greater difference in values of velocity deficit and thus inaccuracy in the bottom half, as the first derivative is greater.

Overall, the model behaves similarily to the power law profile case with respect to its reference case.

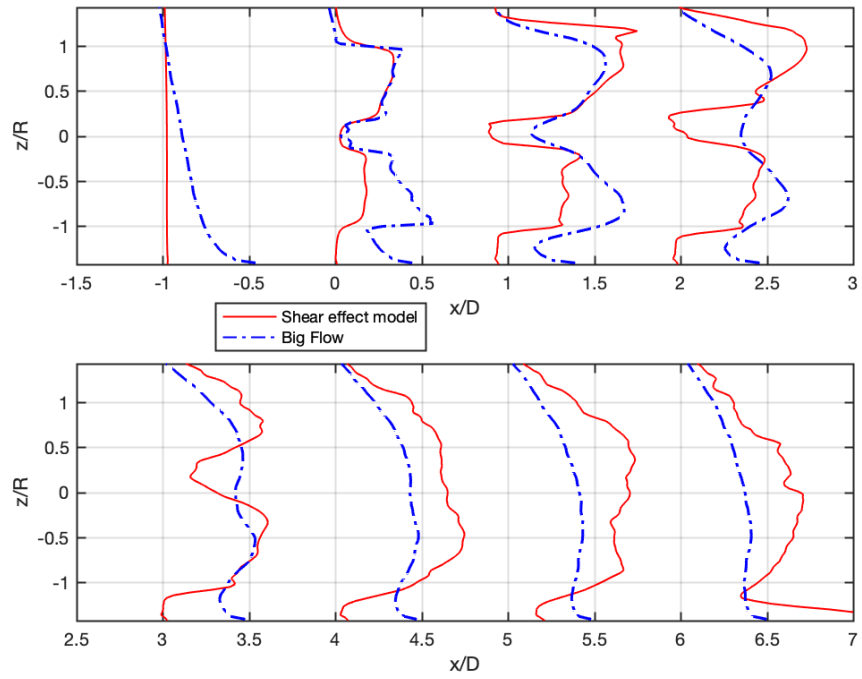

Figure 3.5: Time averaged velocity deficit $\frac{U_\infty - u_x}{U_\infty}$ with complete shear effect modeling versus exact shear with *BigFlow* for an ABL profile.

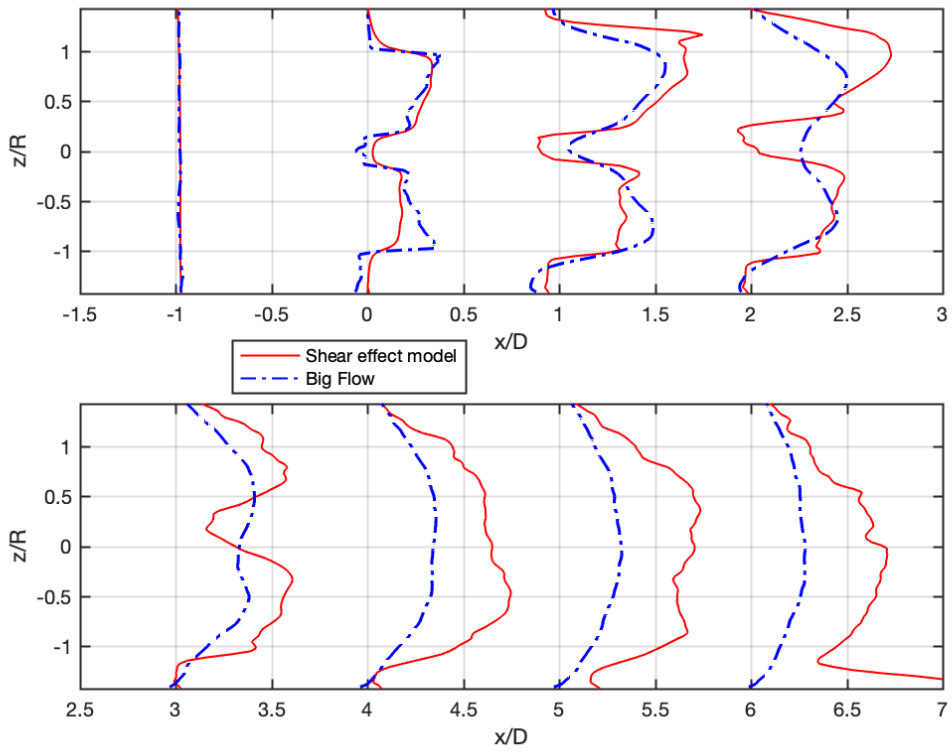

Figure 3.6: Velocity field corrected time averaged velocity deficit $\frac{U_\infty - u_x}{U_\infty}$ with complete shear effect modeling versus exact shear with *BigFlow* for an ABL profile.

3.3 Augmented Power Law

The aim of this section is to investigate where the inaccuracies of the model come from. To do so, the empirical coefficient α of the power law is doubled from its original value of 1/9 to 2/9. This modification will decrease the velocity below the hub while increasing it above as shown in figure 3.7. This has the consequence of increasing the magnitudes of the first and second derivatives (figure 3.8). It is important to note that this increase in the values of the derivatives is not proportional: It doubles the value of the first derivative while slightly increasing that of the second. However, the second derivative remains almost negligeable at hub height in both cases compared to its values close to the ground. Since the 3-D terms all depend on the first derivative while the 2-D term depends on the second, this modification will provide a more complete understanding as to why and how the model reacts to changes in profiles.

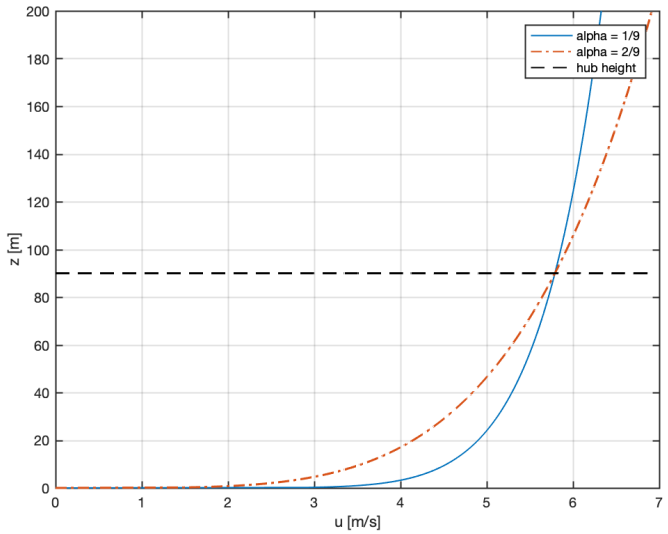

Figure 3.7: Augmented power law velocity profile.

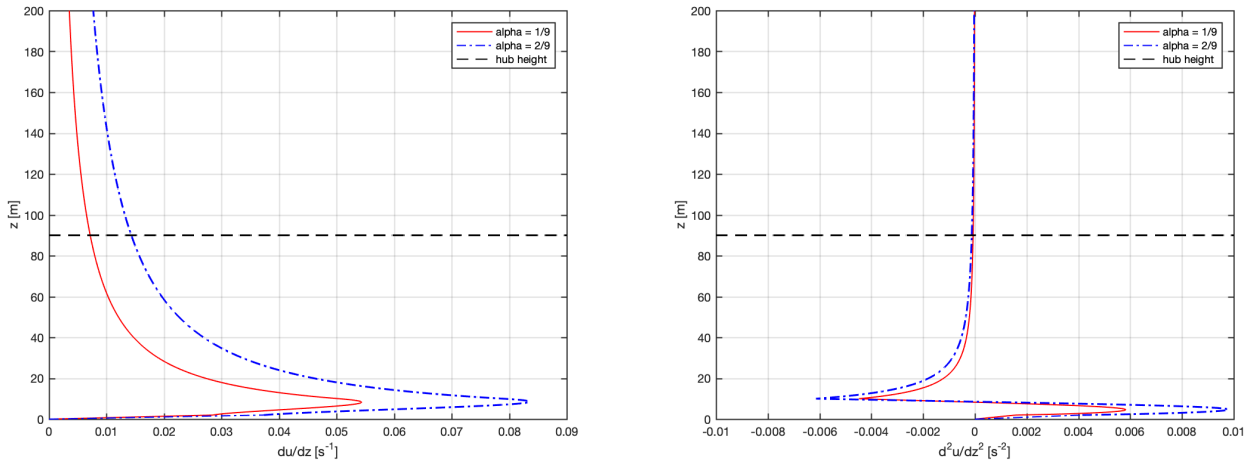

Figure 3.8: First and second derivative profiles with applied masks of the augmented power law.

3.3.1 Results and discussion

Figure 3.9 represents the instantaneous normalized vorticity in the vertical plane for the shear effect model and the exact shear model. The increase in values of the power law's derivative $\frac{dU}{dz}(z)$ is apparent with the red gradient close to the ground. This time, its magnitude in that region is comparable to the one of vorticity generated by the middle section of the blades. The exact shear model shows little reactivity to the modification of the coefficient α. They share the same lack of deviation, caracteristics of the wake center as well as transition into its highly turbulent state. However, in zones of high vorticity, such as the vortex sheet created by the tips of the blades, Kelvin-Helmholtz instabilities are much more defined. Not only do they create larger eddies, the bottom of the vortex sheet generates them closer to the turbine. Since the bottom of the blades is located at $z = 27$m, where the difference in the second derivatives for both alpha coefficients is very small, the behaviour of these eddies appears to be closely linked to the first derivative of the profile and thus the 3-D terms.

However, the shear effect model reacts strongly to the increase in the empirical coefficient. Whereas deflection of the wake was very subtle in the case of $\alpha = 1/9$, here it is more defined and takes different forms depending on the altitude. Kelvin-Helmholtz instabilities begin sooner, at $x/D = 2$. As soon as these form, the bottom of the wake begins deflecting upwards. As opposite vorticity of greater magnitude is formed at the top of the wake, the bottom of the wake is compressed

and shrinks.

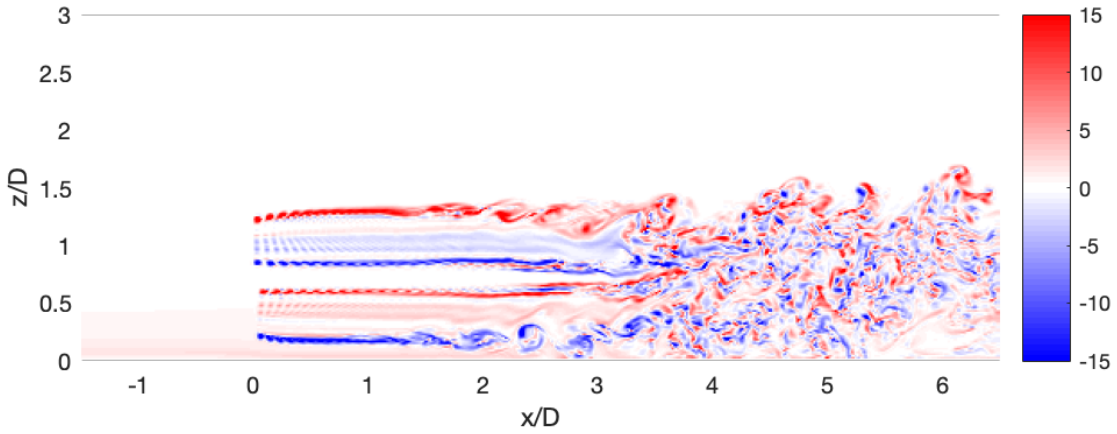

(a) VPM with exact shear modeling

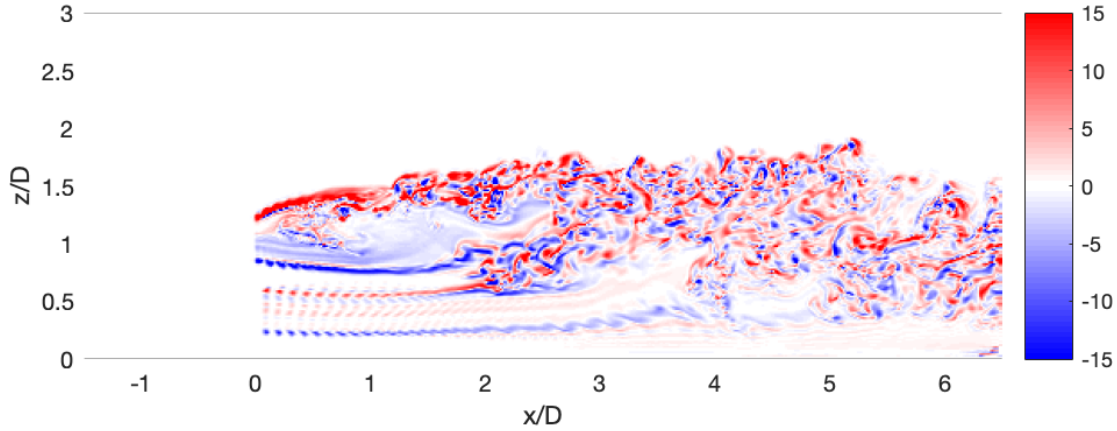

(b) VPM with complete shear effect modelling

Figure 3.9: Instantaneous normalized y-vorticity for the augmented power law profile.

The top of the wake undergoes very chaotic behaviour. Close to the turbine, at $x/D = 1$, a recirculation region forms. This highly physically inaccurate behaviour highlights the discrepancies the model has when dealing with steeper velocity profiles. The vortex sheet at the top of the wake is instantly strongly deviated upwards and breaks up rapidly, due to this recirculation region. This behaviour points to the fact that the 3-D terms are responsible for the over-generation of vorticity (see figure D.1 for a comparison of the velocity deficit profiles of the complete model versus the partial model that is devoid of the 3-D terms). It is

interesting to notice that as soon as the center of the wake is deflected upwards, it becomes highly turbulent. This was the case for $\alpha = 1/9$, although it happened towards $x/D = 3$ instead of $x/D = 2$.

Compared to the case $\alpha = 1/9$, the far wake in the exact shear model simulation is devoid of vorticity close to the ground. The model does respect this behavior, although vorticity progressively increases as it gets further from the ground, until it becomes greater than the exact shear model. So far, the model thus fails even more so than the case $\alpha = 1/9$ to accurately represent the exact scenario as it generates too much vorticity.

The time-averaged streamwise velocities for the different cases are displayed in figure 3.10. The shear effect model creates a very low velocity region of consequent size above the center of the wake near the turbine. This is the consequence of the recirculation region that is linked to the method used to incorporate the wind velocity profile in the lifting lines computational process. At the bottom of the wake, the same yet opposite phenomenon is observed: The flow barely slows down as it passes through the blades beneath the hub.

Above the wake but behind the turbine, the flow is accelerated beyond the value of the uniform velocity field of the particles upstream of the turbine. In the far wake, the pattern of the low and high velocity regions of the flow roughly matches that of the exact shear model. However, the values are inaccurate and the flow is much too slow due to the excesst of turbulence generated by the shear effect model.

For the sake of comparison, a velocity corrected version of the streamwise velocity field of the exact shear model is also depicted. The flow matches even less than without correction, but gives an idea of the difference of values the wake above and beneath the hub should see in terms of velocity. The shear effect model undergoes so little deceleration past the turbine that it doesn't expand. Its far wake is deflected downwards, unlike in the reference case.

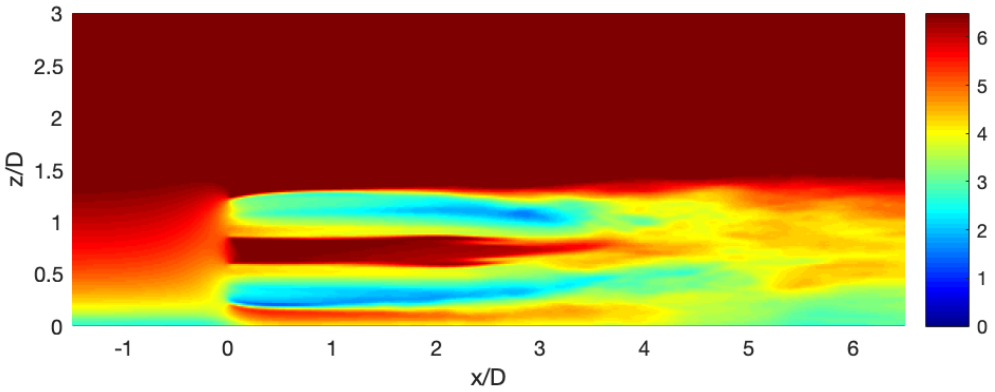

(a) VPM with exact shear modeling.

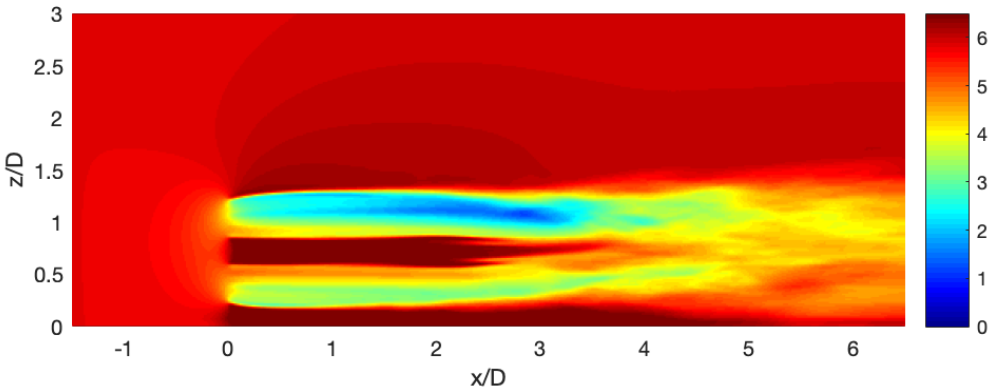

(b) VPM with exact shear modeling and applied velocity field correction.

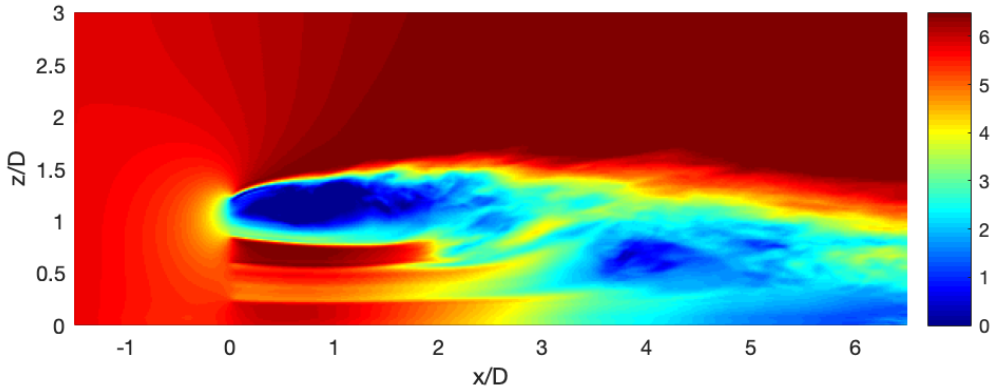

(c) VPM with complete shear effect modeling

Figure 3.10: Time averaged streamwise velocity for the augmented power law profile.

Finally, velocity deficit plots are presented in figure 3.11. Through this figure, it becomes apparent that the model creates the opposite effect it should. The velocity deficit increases above hub height and decreases below, even more so than in the case with $\alpha = 1/9$. The uncorrected velocity deficit plot of the exact shear model demonstrates the opposite behaviour.

The corrected velocity deficit of the exact case shows that its values above hub height become greater than its values below. This was not the case for $\alpha = 1/9$. This implies that with sufficient steepness in the velocity profile, subtracting it from the velocity field behind the turbine becomes less efficient at recreating a symmetrical behaviour in terms of velocity magnitude that would have occured without shear.

Whereas in the case $\alpha = 1/9$ the partial and complete shear effect models shared an almost identical behaviour in the near wake, here they rapidly grow different from one another. This highlights the way the effect of the 3-D terms increases drastically with an increase in the first derivative of the profile, and provides quantification in terms of their effect relative to the 2-D term. The 3-D terms are responsible for the upwards deviation of the low velocity region. At this point, both versions of the shear effect model are highly inaccurate. In the case of $\alpha = 1/9$, the profiles were still comparable albeit their orders of magnitude wrong.

The velocity deficit plots highlight the fact that the discrepancies in the model are not just linked to the 3-D terms generating too much vorticity. The differences in values in both the corrected and uncorrected figures point towards the fact that the uniform velocity field of the particles upstream of the turbine has too large of an impact on the way vorticity is created at the turbine. Even when the lifting lines method is adjusted use the shear velocity profile, the fact that the effect of the blades are stacked on a velocity field not conform to the reality it attempts to model changes the whole way the NS equations process the vorticity field.

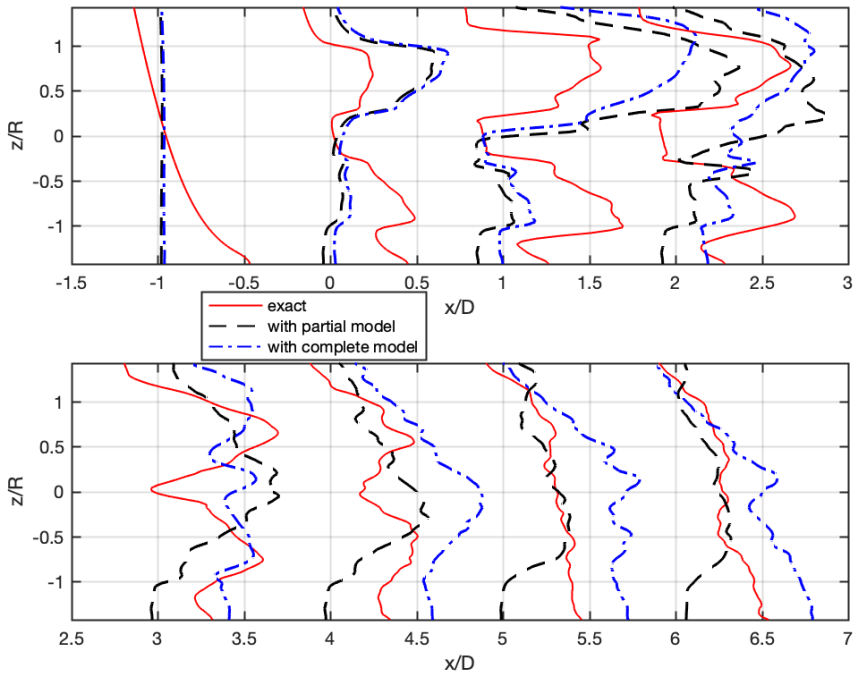

(a) Without velocity field correction.

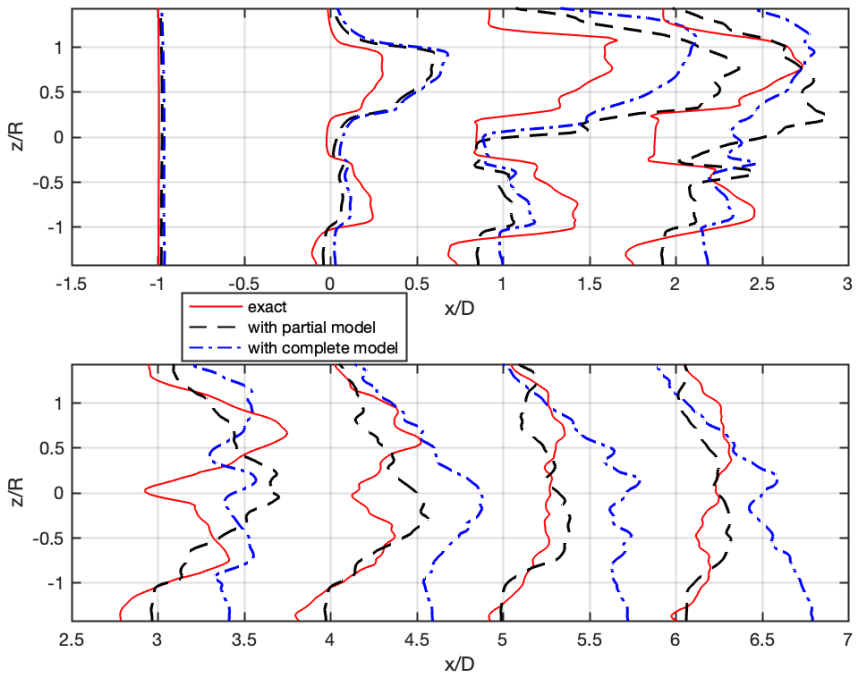

(b) With velocity field correction applied to exact VPM case.

Figure 3.11: Time averaged velocity deficit $\frac{U_\infty - u_x}{U_\infty}$ with exact shear, partial shear effect modeling and complete shear effect modeling for the augmented power law profile.

Conclusion

The main objectives of this Master's thesis were (1) to understand where and how the shear effect model acted and (2) to determine its accuracy with respect to physically accurate reference cases, while providing clear visualisations to support the explanatory process. The basis of the shear effect model is based on the assumption that the vorticity due to the shear velocity profile does not interact with vorticity generated by the turbine, allowing to model the effect of the shear velocity profile solely by adding terms to the NS equations.

Chapter 2 assessed the effects of the shear effect model by comparing it to a version of the VPM method with an adjusted lifting lines method. This adjusted lifting lines method acted on the shear velocity profile despite the uniform velocity of the particles upstream of the turbine. It was found to have drastic effects on the flow : the vorticity shed based on the shear velocity profile is not compensated by a corresponding particles velocity field. When modeling a linear shear velocity profile, only the 3-D terms that depend of the first derivative of the velocity profile are non-zero. These terms were found to accelerate the flow above hub height and slow it down below.

Then, a power law velocity profile was modeled. A variant of the shear effect model with all 3-D terms omitted was created to better observe the effect of the 2-D term, which is a function of the second derivative of the wind velocity profile. Contrarily to initial expectations, this term was found to have very little impact on the flow, especially in the near wake. In the far wake, it slows the flow near the ground down.

When comparing to *exact* references cases, the model was found to generate too much vorticity above hub height and too little below. This discrepancy happens at the blades and is caused by the lifting lines correction, rendering the entire modeled flow inaccurate. Due to this phenomenon, the model's wake center sees an upwards deflection not present in the reference flow's case. A correction was applied to the entire domain of the exact reference cases to match the model's particle's uniform velocity field. While decreasing the difference in velocity magnitudes in

the near wake, the correction creates strong discrepancies near the ground, as the model acts strongly on this region. The augmented power law showed greater differences between the partial and complete shear effect model, implying the 3-D terms react strongly to an increase in steepness. This augmented profile increases the inaccuracy of the model and the discrepancies creates by the lifting lines model at the blades.

There is still research worthy of being carried out about the shear effect model. A 2015 article[3] presented a version of the model without the lifting lines correction applied in this work, which although physically inaccurate, yielded more coherent results (see Appendix B). Finding a better correction to apply to the lifting lines method could significantly improve the model. Furthermore, in NTF and power law conditions, a mask was applied near the ground to prevent the asymptotic behaviour of the derivatives to generate an excess of vorticity. To decrease the effect of this source of inaccuracy, turbine simulations with blades further from the ground could be performed. A better solution would be to include wall modeling within the VPM method. Finally, the model showed signs of varying degrees of accuracy depending on the value of the empirical coefficient α of the power law. A parametric study of this coefficient could establish for which profiles the model is more accurate.

Appendix

Appendix A

Slices of velocity in the x-plane without shear velocity profile modeling

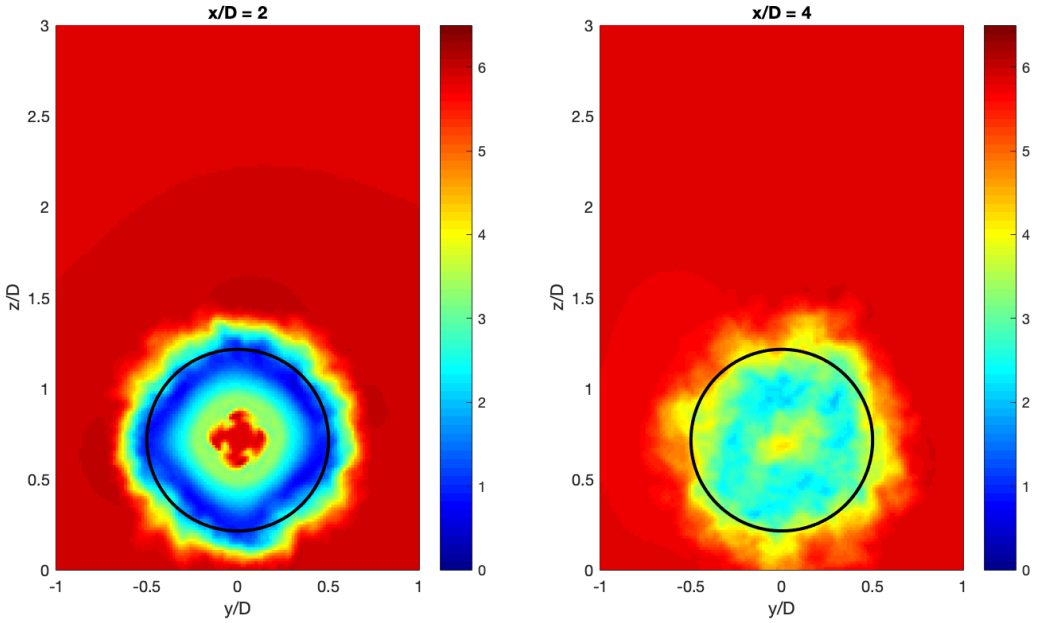

Figure A.1: Time-averaged streamwise velocity in the y-z plane without lifting lines correction or shear effect modeling. The flow is axisymmetric around the turbine's streamwise axis.

Appendix B

Comparison to Nordtank 500kW turbine w/ unbounded & linear conditions

In 2015, Emmanuel Branlard developped his own version of the shear effect model that ran on a VPM method [3]. Vorticity iso-contours of the results of his shear effect model at $t = 300$s of simulation time are shown in figure B.1. The depicted dashed contour represents an erroneous version of the model presented in his article, while the black dashed lines correspond to the correct version that this paper presents.

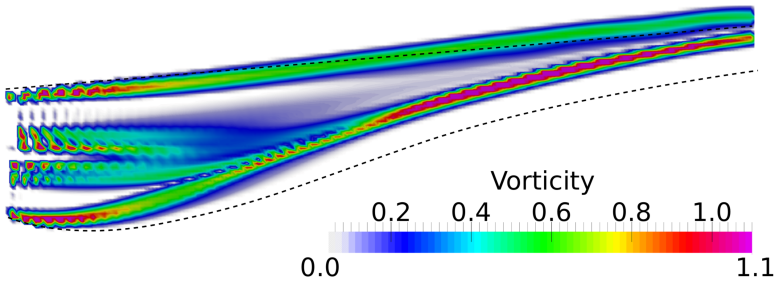

Figure B.1: Vorticity iso-contours in the wake of the Nordtank 500kW turbine.

His simulation models the three-bladed Nordtank 500kW stall regulated wind turbine, with a rotational speed of $\Omega = 27.1$RPM and a free-stream velocity of $U_0 = 7.5$m/s. With a turbine diameter of $D = 41$m, this yields a tip-speed ratio of $\lambda = 7.7$. The shear is linear of slope $\frac{dU}{dz} = 0.079[ms^{-1}]$. To mimic this behaviour with the VPM shear effect model developed in this paper, the latter is adimensionalized appropriately to the tip-speed ratio. The rotational speed of

the NREL-5MW offshore wind turbine is set to $\Omega = 10.3$RPM, yielding a free-stream velocity of $U_0 = 8.82$m/s and a linear shear of slope $\frac{dU}{dz} = 0.0302[ms^{-1}]$. The vorticity iso-contours of this simulation are presented in figure B.2. In this configuration, the shear effect model demonstrates highly chaotic and unstable behaviour. In fact, it never converges to a stable state as vorticity keeps stacking up.

The simulations are not at all coherent with one another. However, there are many differences between the two configurations. The three-bladed Nordtank 500kW simulations differs from the NREL-5MW in the following ways:

- There is no correction applied at the blades to generate vorticity according to the profile it is supposed to model.
- It is an inviscid flow (viscous term in NS equations equal to 0).
- It has different blade profiles that aren't corrected by adimensionalization.
- It has a different hub diameter.

Similar results to the Nordtank simulation were obtained with an erroneous version of the VPM shear effect model while it was still in development. The mistake was that the sign was inverted in the computation of the shear vorticity as such:$\boldsymbol{\Omega} = \nabla \times \mathbf{U} = -\frac{dU}{dz}(z)\mathbf{e}_y$.

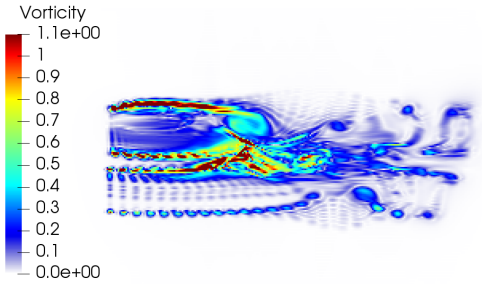

(a) Simulation at t=50s.

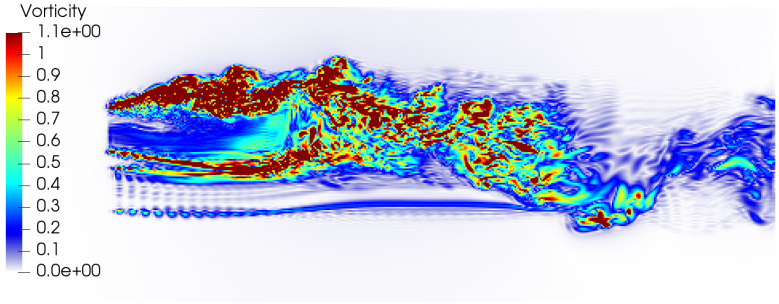

(b) Simulation at t=100s.

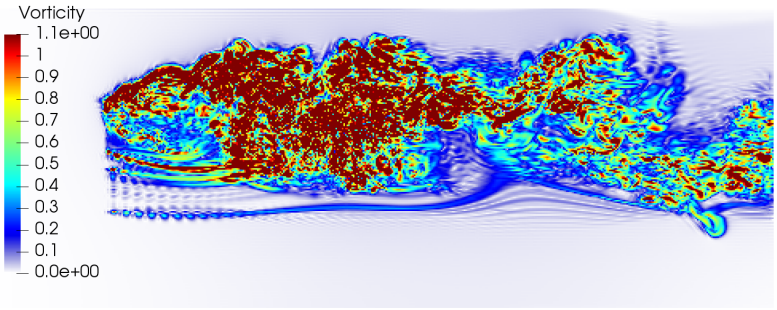

(c) Simulation at t=150s.

Figure B.2: Vorticity iso-contours in the wake of the NREL-5MW turbine.

Appendix C

Coles composite profile

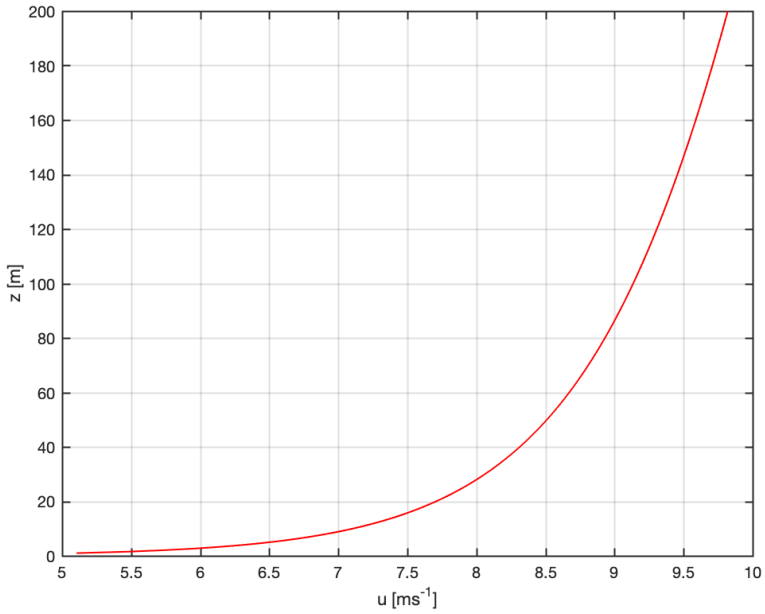

Figure C.1: Velocity of the Coles composite profile.

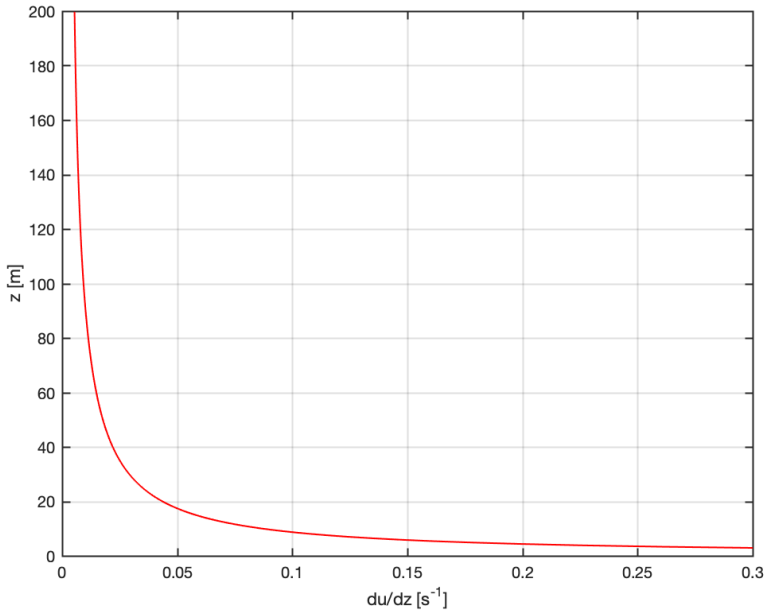

Figure C.2: First derivative of the Coles composite profile.

Appendix D

Partial vs. Complete model for augmented shear profile

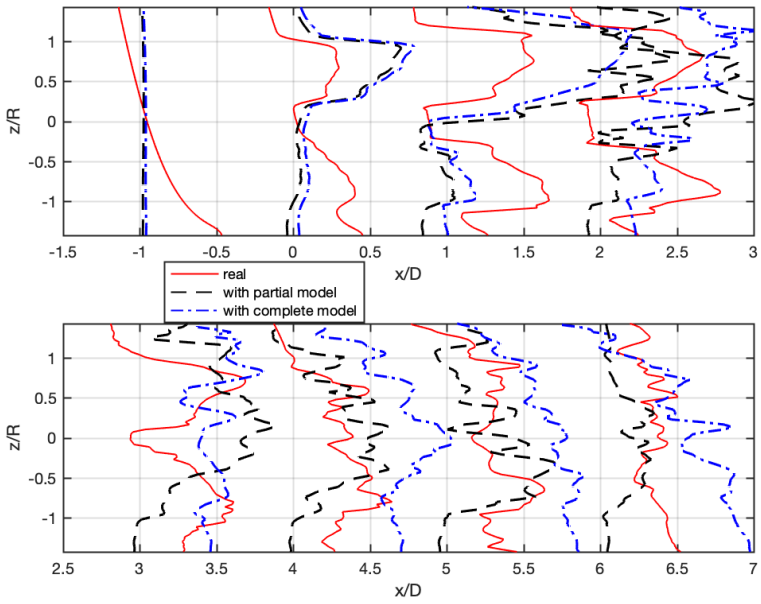

Figure D.1: Streamwise velocity deficit profiles of the exact case, partial model and complete model with augmented shear velocity profile.

Bibliography

[1] Stephane Backaert, Philippe Chatelain, and Gregoire Winckelmans. Vortex particle-mesh with immersed lifting lines for aerospace and wind engineering. *Procedia IUTAM*, 18:1–7, 12 2015.

[2] Emmanuel Branlard. *Wind Turbine Aerodynamics and Vorticity-Based Methods*. Springer International Publishing, Gewerbestrasse 11, 6330 Cham, Switzerland, 2017.

[3] Emmanuel Branlard, George Papadakis, M Gaunaa, Gregoire Winckelmans, and Torben Larsen. Aeroelastic large eddy simulations using vortex methods: unfrozen turbulent and sheared inflow. *Journal of Physics: Conference Series*, 625, 06 2015.

[4] Denis-Gabriel Caprace, Grégoire Winckelmans, and Philippe Chatelain. An immersed lifting and dragging line model for the vortex particle-mesh method. *Theoretical and Computational Fluid Dynamics*, Jan 2020.

[5] Philippe Chatelain, Alessandro Curioni, Michael Bergdorf, Diego Rossinelli, Wanda Andreoni, and Petros Koumoutsakos. Billion vortex particle direct numerical simulations of aircraft wakes. *Computer Methods in Applied Mechanics and Engineering*, 197(13):1296 – 1304, 2008.

[6] Philippe Chatelain and Petros Koumoutsakos. A fourier-based elliptic solver for vortical flows with periodic and unbounded directions. *J. Comput. Physics*, 229:2425–2431, 2010.

[7] R. Cocle, L. Bricteux, and G. Winckelmans. Scale dependence and asymptotic very high reynolds number spectral behavior of multiscale subgrid models. *Phys. Fluids*, 21, 2008.

[8] Roger Cocle, Gregoire Winckelmans, and Goeric Daeninck. Combining the vortex-in-cell and parallel fast multipole methods for efficient domain decomposition simulations. *Journal of Computational Physics*, 227:9091–9120, 11 2008.

[9] Chaouki Ghenai. *Life Cycle Analysis of Wind Turbine*. 02 2012.

[10] Martin O. L. Hansen. *Aerodynamics of Wind Turbines, Second Edition*. Earthscan, 8–12 Camden High StreetLondon, NW1 0JH, UK, 2008.

[11] S. A. Hsu, Eric A. Meindl, and David B. Gilhousen. Determining the power-law wind-profile exponent under near-neutral stability conditions at sea. *Journal of Applied Meteorology*, 33(6):757–765, 1994.

[12] IEA. Renewables 2019. *IEA*, 197, 2019.

[13] Jonkman JM, S. Butterfield, W. Musial, and G. Scott. Definition of a 5mw reference wind turbine for offshore system development. *National Renewable Energy Laboratory (NREL)*, 01 2009.

[14] Rachel Leuthold. *Multiple-Wake Vortex Lattice Method for Membrane-Wing Kites*. PhD thesis, 12 2015.

[15] Yves Marichal. *An immersed interface vortex particle-mesh method*. TFL, Place du levant, 2014.

[16] Rupert Storey. *Large Eddy Simulation of Dynamically Controlled Wind Turbine Arrays*. PhD thesis, 08 2014.

[17] G. S. Winckelmans. *Vortex Methods*, pages 1–24. American Cancer Society, 2017.

[18] J. Z. Wu and J. M. Wu. Vorticity dynamics on boundaries. *Advances in Applied Mechanics*, 32:119 – 275, 1996.

Abbreviations

ABL	Atmospheric Boundary Layer
CFD	Computational Fluid Dynamics
LES	Large-Eddy Simulation
MPI	Massively Parallel Architectures
NS	Navier-Stokes
NTF	No-Through Flow
ODEs	Ordinary Differential Equations
PDEs	Partial Differential Equations
RK3	Third Order Runge-Kutta
SGS	Sub-Grid Scale
TFL	Thermodynamics and Fluid mechanics Lab
UCL	Universite Catholique de Louvain
VPM	Vortex Particle-Mesh

UNIVERSITÉ CATHOLIQUE DE LOUVAIN
École polytechnique de Louvain
Rue Archimède, 1 bte L6.11.01, 1348 Louvain-la-Neuve, Belgique | **www.uclouvain.be/epl**